Development of ionophore hydrogen-bonded organic frameworks composed of crown ether derivatives

(クラウンエーテル誘導体で構成されるイオノフォア水素結合性有機フレームワークの開発)

北海道大学大学院環境科学院

Xin Chen

Acknowledgement

This thesis has been carried out under the direction of Professor Ichiro Hisaki between October 2018 and September 2021 at Graduate School of Environment Science, Hokkaido University.

At the very first, I am honored to express my deepest gratitude to Professor Ichiro Hisaki, with whom careful guidance, precious suggestions, and persistent encouragements during this work.

I would like to express my sincere gratitude to Professor Takayoshi Nakamura for his kind suggestions and warm encouragements. I owe special thanks to Assistant Professors Kiyonori Takahashi and Kilingaru I. Shivakumar for their inspired suggestions and hearty encouragements.

I am grateful to Professor Shin-ichiro Noro, Assistant Professor Kenta Kokado, Assistant Professor Rui-kang Huang and Assistant Professor Cheng Xue for their for their kind technical supports and advices. I am also extremely grateful to Professors Yoshimitsu Sagara (Tokyo Institute of Technology) and Nobuyuki Tamaoki for purification of compounds by preparative HPLC. I am thankful to Doctors Kunihisa Sugimoto and Nobuhiro Yasuda at SPring-8 for collection of X-ray diffraction data.

Furthermore, acknowledgements are to all other members of Professor Nakamura's laboratory, Professor Hisaki's laboratory and Professor Noro's laboratory for their friendship and encouragements. Special thanks to Miss. Qin Ji, Mr. Jia-bing Wu, Mr. Zhu-xi Yang, Dr. Si-min Li and Dr. Xin Zheng for their warm encouragement in my research and daily life.

The author is indebted for the financial support of Chinese Scholarship Council (CSC) for financial support.

At last but certainly not least, I would like to exhibit deep appreciation to all my family members, especially my parents, Mr. Chun-ping Chen and Mrs. Hui-hui Dou for constant understanding, financial supports and affectionate encouragements.

Xin Chen

Graduate School of Environment Science

Hokkaido University

September 2021

Contents

List of Tables

PAGE

List of Schemes

PAGE

List of Figures

PAGE

Chapter 1

General introduction

1-1. Proton conductive crystalline porous materials

Crystalline porous materials include metal–organic frameworks (MOFs), coordination polymers (CPs), polyoxometalates (POMs) and covalent organic frameworks (COFs), which have attracted many concerns in the field of proton-conducting materials. The designable structures and high surface areas of these materials offer tremendous opportunities for orderly accommodation of proton carriers and the systemically modification of their concentration and mobility in available spaces. Based on the understanding of the relationship between the structure and proton conductivity, controllable synthesis of porous materials with high proton conductivity will gradually be achieved. The proton exchange membrane fuel cell (PEMFC) is of particular interest owing to fast transportation and ease of handling. Most of the porous crystalline PEMs that have been tried and tested are either inorganic materials, MOFs, or more recently COFs. However, hydrogen-bonded organic frameworks (HOFs) have emerged as a new class of porous crystalline material systems with the great natures of easy synthesis, structural elucidation by single-crystal X-ray diffraction, low-energy regeneration processes, and good thermal stability, which can be a great candidate in fuel-cell industries are rarely explored.

In addition, crown ethers with an excellent ability to bind alkali metal cations and water molecules, is always a hot research topic as an ion conductive material. Moreover, theoretical calculation suggested that dibenzo-18-crown-6 with H_3O^+ ions located in the cavities of the crown ether interact with water molecules. Therefore, crystalline frameworks composed of crown ethers are expected to show the proton conductivity. However, proton conductive HOFs based on crown ethers are hitherto unknown. In this thesis I newly designed 18-crown-6 derivatives with several 4,4'-dicarboxy-*o*-terphenyl (CT) groups, as the building block molecules to develop proton conductive HOFs.

1-2. A brief history of proton conduction

The increasing energy demands of the world required a new clean alternative energy system to maintain the concept of green sustainable concept such as fuel cells (FCs).[1-3] FCs have the electrochemical properties that can promote chemical energy to electrical energy without carbon emission at high thermodynamic efficiencies to solve the issue of the environment. All advantages of FCs have driven researchers to explore for proton conducting materials based on conductive polymers, which is the heart of the of fuel cell technology.

Nafion[4] discovered in the 1960s, as the first proton-conducting material exploited for applications in FCs, which operates excellent conductivity in the presence of water and at the temperature lower than 80 ºC. However, the high cost and low operation temperature prevent the larger-scale use in many fields. Furthermore, it is tough to optimize the proton transport pathway.

With persistent research several intrinsic proton conducting materials[5-6] which show significant impact on the increasing in conductivity have been explored, while the amount of this kind of conductors is limited. $CsHSO_4$[6] as a discrete ionic crystal is a good proton conductor at intermediate temperatures, but it is readily soluble in water, which limits its application in FCs.[7] On the other hand, some composite materials based on its family, such as $CsHSO_4$–SiO_2 and CsH_2PO_4–SiO_2,[8-9] exhibit superior proton conductivity, which operate at a very high temperature that in range of 600–1000 ºC and show a conductivity range of 10^{-2}–10^{-6} S cm^{-1}. In addition, the fact of strong acids and heterocyclic organic molecules, such as organic sulphonates, imidazole and pyrazole employed as additives in polymers with high proton conductivity indicates that organic conductive polymers are promising candidates. This approach can enhance the conductivity and thermal and chemical stability.

In addition, polybenzimidazole membranes impregnated with phosphoric acid (PBI)[6] have attracted much attention due to the intermediate operation temperature (80–200 ºC) and the high proton conductivity values 10^{-2} S cm^{-1} comparable to Nafion. These days, strong acids and heterocyclic organic molecules, such as organic sulphonates,[10] imidazole and pyrazole,[11-12] have been employed as additives in polymers. The combination of organic molecules with these polymers produces novel materials with interesting proton-conducting behaviors as well as this approach can enhance the conductivity and thermal and chemical stability. Nevertheless, it is still a big challenge to investigate crystalline networks with proton conductivity. Heteropoly acids (HPAs) are ideal candidates for proton-conducting electrolytes because of their unique characteristics of fast charge-transfer and abundant proton containers. The proton conduction of two Keggin heteropoly compounds, $H_3PM_{12}O_{40}\cdot 29H_2O$ (M = Mo, W), was firstly reported by Nakamura in 1979.[13] Recently, several POM-based MOFs were also reported.[14-17] As a critical class of functional crystalline materials, MOFs with high surface areas, high porosities and extended crystalline structures result in a new platform for proton-conducting materials. Water mediated proton-conducting MOFs and anhydrous proton conducting MOFs as two representative proton-conducting MOFs have been studied. The water-mediated MOFs are limited to use at low temperature (20–80 ºC), with proton conductivity ranging between 10^{-2} and 10^{-8} S cm^{-1}, whereas the anhydrous MOFs operate at an intermediate temperature (100–250 ºC). Several achievements have been known,[18-20] however, MOFs suffer from poor stability, which limits their applicability under fuel cell operating conditions. During these years, COFs have emerged as a new class of crystalline materials via covalent ligation of lighter elements (e.g., B, C, N, O) in a periodic manner. COFs possess the following advantages: relatively lightweight, various functionalities, high stability, and a high degree of internal ordering. These features make COFs attractive for proton conduction. In 2014, the first emergence of COFs as proton-conducting materials was reported, showing moderate proton conductivity values.[21] Accurate structural information of the

crystalline network sheds light on the proton-conduction pathway and mechanism, and the tunable structures of the crystalline network can improve the proton-conducting properties. Herein, chemists highlight the developments in new crystalline networks and related materials.

1-3. Proton-conducting mechanism

There are two principal mechanisms related to the transport of protons, namely, the Grotthuss and vehicular mechanisms.[22-23] The Grotthuss mechanism establishes the conduction of protons within an infinite network of hydrogen bonds. Firstly, by means of water molecules, the protons transfer within hydrogen bonds from one water molecule to another. Secondly, additional reorientation of neighboring water molecules results in the formation of a continuous trajectory for proton migration. In other words, the protons pass along the hydrogen bonds. The vehicular mechanism involves the movement of protons via the assistance of a moving vehicle (e.g., H_2O, NH_3). The protons diffuse with the vehicles, while unloaded vehicles move in the opposite direction. The activation energies obtained from ac impedance data can be used to distinguish the two types of processes. The Grotthuss mechanism based conduction processes generally involve the cleavage of hydrogen bonds (approximately 0.11 eV),[24] so the activation energies (Ea) are lower than 0.4 eV. In the vehicular mechanism, transfer of larger vehicles (e.g., H_3O^+, NH_4^+) requires a larger energy, and the energies (Ea) are usually larger than 0.4 eV.

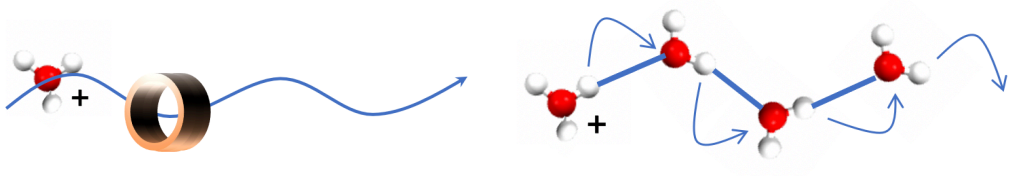

Figure 1-1. Two types of proton diffusion motion: vehicle and Grotthuss mechanism.

Naturally, the two processes can be identified via the activation energies which can be determined by a combination of structural analysis and conductivity. Actually, proton conductivity is evaluated by alternating current (AC) electrochemical impedance spectroscopy (EIS) measurement in a wide frequency range using a single crystal or pelletized powder and follows the equation:[22]

$$\sigma = \frac{\mathrm{n(Ze)^2D}}{kT}\exp(-\mathrm{E_a}/kT)$$

where σ is conductivity, n, Ze, D, Ea, k, T are carrier concentration, charge of the conducting carrier, self-diffusion coefficient, activation energy, Boltzmann constant, and temperature, respectively.

1-4. Proton conduction in porous materials

Crystalline porous materials such as MOFs, POMs, COFs, HOFs, POM-based MOFs/CPs and COF composite materials have been used for proton conduction, especially MOFs. The structural characteristics of crystalline porous materials are promising for the design of proton conductors. Chemists are focus on improving materials for FCs, they consider it significant to achieve high proton conductivity, sufficient thermal/chemical stability, and flexibility. Compared with conventional materials, a unique characteristic of crystalline porous materials for proton conductivity is the coexistence of designable structures and tailorable chemistries, which provide an opportunity to study the proton-conduction pathway and to further optimize the proton-conduction properties. Chemists believe that advances made in the structural chemistry of crystalline porous materials will contribute to creating a new class of solid proton conductors.

Since the first proton-conductive MOF, copper dithiooxamidate ((HOC_2H_4)2dtoaCu) and its derivatives, investigated by Kanda in 1979,[25] followed by

Kitagawa and Nagao.[26-27] much progress has been achieved in this field.[28-31] The self-assembled frameworks assisted by coordination bonds can introduce various guest molecules into proton-conducting frameworks. Based on the strategies for achieving proton conductive MOFs in previous reports, proton-conductive MOFs can be divided into five categories as shown in Figure 1-2 related to the proton source and jumping site types of proton-conductive MOFs.[32] (i) counterion inclusion such as hydronium (H_3O^+), ammonium (NH_4^+, $Me_2NH_2^+$), or anion (SO_4^{2-});[28,33-35] (ii) functionalized structural components such as noncoordinated functional groups in organic ligands (e.g., phosphonate, sulfonate, carboxylate and hydroxylate);[36-37] (iii) coordinative insertion of functional molecules in metal centers (H_2O, EtOH, and imidazole);[38-41] (iv) the inclusion of functional guest molecules such as acid molecules, protic organic molecules, POMs, or metal−organic polyhedral (MOP) molecules, constitutes the simplest method of using MOF porosity;[38,42−43] (v) consistent of the intrinsic and extrinsic defective MOFs for proton conduction.[44−46]

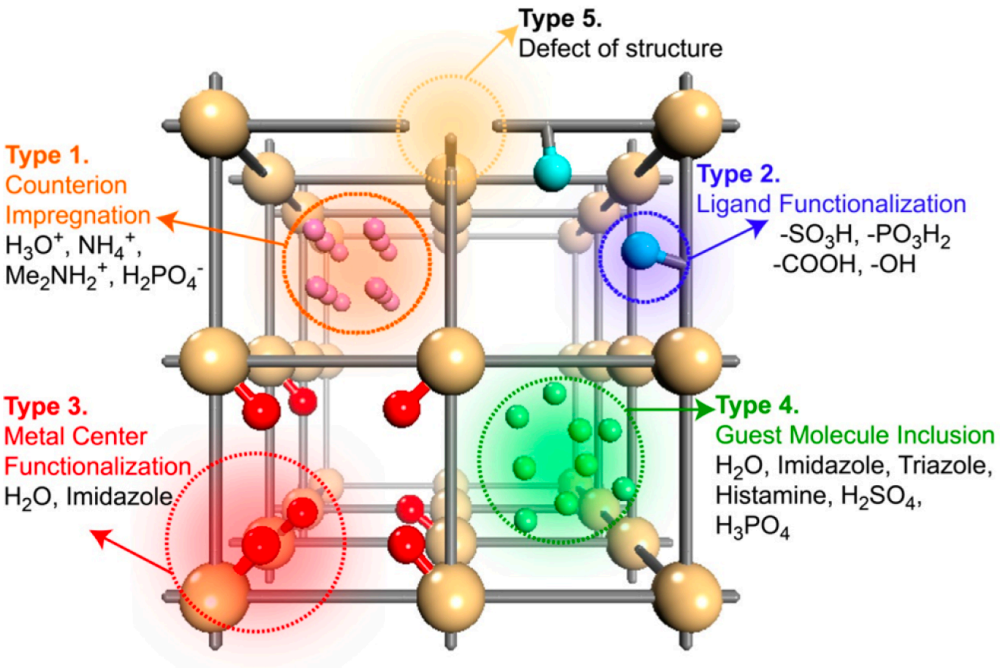

Figure 1-2. Classification of the types of proton-conducting MOFs. Copyright by 2020 American Chemical Society

In addition, most hitherto proton-conducting porous materials have been summarized in the table 1-1.

Table 1-1. Summary of proton-conducting porous materials.

MOFs/CPs	Conductivity (S cm^{-1})	E_a (eV)	Temperature/ humidity	Conducting medium
$(NH_4)_3[CO_2(bamdpH)_2(HCOO)(H_2O)_2]$	8.0×10^{-6}	0.69	T = 25 ºC, 95 % RH	H_2O, $-PO_3H$, NH_4^+
CoLa-II$[CoLa(notpH)(H_2O)_6]ClO_4 \cdot 5H_2O$	3.5×10^{-6}	0.34	T = 25 ºC, 95 % RH	H_2O, $-PO_3H$, ClO_4^-
PCMOF3	3.5×10^{-5}	0.17	T = 25 ºC, 95 % RH	H_2O, $-PO_3H$
PCMOF10	3.5×10^{-2}	0.40	T = 25 ºC, 95 % RH	H_2O, $-PO_3H$, $-COOH$
Li-HPAA:$[Li_3(OOCCH(OH)PO_3)$-$(H_2O)_4] \cdot H_2O$	1.1×10^{-4}	0.84	T = 24 ºC, 98 % RH	H_2O, $-PO_3H$, $-COOH$
Na-HPAA:$Na_2(OOCCH(OH)PO_3H)$-$(H_2O)_4$	5.6×10^{-3}	0.39	T = 24 ºC, 98 % RH	H_2O, $-PO_3H$, $-COOH$
K-HPAA:$K_2(OOCCH(OH)PO_3H)$-$(H_2O)_2$	1.3×10^{-3}	0.98	T = 24 ºC, 98 % RH	H_2O, $-PO_3H$, $-COOH$
Cs-HPAA:Cs(OOCCH(OH)-PO_3H)	3.5×10^{-5}	0.40	T = 24 ºC, 98 % RH	H_2O, $-PO_3H$, $-COOH$
H_3PO_4@MIL-101	3.0×10^{-3}	0.25	T = 150 ºC	H_3PO_4
PCMOF-17	1.2×10^{-3}	0.31	T = 25 ºC, 40 % RH	H_2O, $-SO_3H$, Me_2NH_2
$\{[Zn(bpeH)(5\text{-}sip)(H_2O)] \cdot (H_2O)\}_n$	2.5×10^{-6}	0.54	T = 65 ºC, 95 % RH	H_2O, $-SO_3H$
$\{[Cu(pyz)(5\text{-}Hsip)(H_2O)_2] \cdot (H_2O)_2\}_n$	3.5×10^{-5}	0.35	T = 65 ºC, 95 % RH	H_2O, $-SO_3H$
$\{[Cu(bpee)_{0.5}(5\text{-}sip)(H_2O)_2] \cdot (H_2O)_4(bpeeH_2)_{0.5}\}_n$	9.9×10^{-8}	0.40	T = 65 ºC, 95 % RH	H_2O, $-SO_3H$
$\{[Cu(bpy)(5\text{-}Hsip)(H_2O)] \cdot (H_2O)\}_n$	5.8×10^{-6}	0.43	T = 65 ºC, 95 % RH	H_2O, $-SO_3H$
UiO-66(Zr)-SO_3H	0.3×10^{-2}	0.27	T = 30 ºC, 97 % RH	H_2O, $-SO_3H$
H_2SO_4@MIL-101(Cr)	1.0×10^{-2}	0.42	150 ºC	H_2SO_4
H_2SO_4@MIL-101-SO_3H	1.82	0.21	T = 70 ºC, 90 % RH	H_2O, H_2SO_4
	0.9×10^{-2}		−40 ºC	
PCMOF2 1/2(Tz)	1.17×10^{-1}	0.22	T = 85 ºC, 90 % RH	H_2O, $-SO_3H$, $-PO_3H$, Tz
PCMOF2 1/2(Pz)	1.11×10^{-1}	0.16	T = 85 ºC, 90 % RH	H_2O, $-SO_3H$, $-PO_3H$, Pz
UMOM-100-b (MOP@PCN-777)	2.1×10^{-6}	0.66	T = 80 ºC, 90 % RH	H_2O, $-SO_3H$, $-COOH$
MIL-53(Fe)	2.0×10^{-5}	0.21	T = 25 ºC, 95 % RH	H_2O, $-COOH$
	0.7×10^{-5}		T = 80 ºC, 95 % RH	
MIL-53(Al)-$(COOH)_2$	4.9×10^{-7}		NH_3 100kPa	NH_3, $-COOH$
UiO-66(Zr)-COOH	1.0×10^{-3}	0.18	T = 30 ºC, 97 % RH	H_2O, $-COOH$
	2.3×10^{-3}	0.17	T = 90 ºC, 95 % RH	
BUT-83	3.9×10^{-2}	0.34	T = 80 ºC, 97 % RH	H_2O, $-COOH$
PCMOF-20	1.0×10^{-2}	0.20	T = 80 ºC, 95 % RH	H_2O, $(Me_2NH_2)^+$
CPM-103a	2.3×10^{-3}	0.66	T = 22.5 ºC, 98 % RH	H_2O, $Himdc^{2-}$
CPM-103b	2.1×10^{-3}		T = 22.5 ºC, 98 % RH	H_2O, $Himdc^{2-}$
$NMe_3(CH_2COOH)$ [$FeCr(ox)_3$]	8.0×10^{-4}		T = 25 ºC, 65 % RH	$NMe_3(CH_2COOH)$ H_2O
$NEt_3(CH_2COOH)$ [$MnCr(ox)_3$]	1.0×10^{-7}		T = 25 ºC, 60 % RH	$NEt_3(CH_2COOH)$ H_2O

$NBu_3(CH_2COOH)$ $[FeCr(ox)_3]$	2.0×10^{-11}		*T* = 25 ºC, 60 % RH	$NBu_3(CH_2COOH)$ H_2O
POM-OF	1.0×10^{-2}	0.22	*T* = 80 ºC, 75 % RH	H_2O, Na^+, $[(n\text{-}Bu)_4N]^+$
LnMOF-1	1.1×10^{-5}		*T* = 20 ºC, 90 % RH	H_2O
	2.1×10^{-3}		150 ºC	
*bio*MOF	8.6×10^{-4}	0.34	*T* = 80 ºC, 95 % RH	H_2O
MIL-53(Al)	2.3×10^{-8}		*T* = 25 ºC, 95 % RH	H_2O, NH_3
	3.6×10^{-7}	0.47	*T* = 80 ºC, 95 % RH	
	9.1×10^{-11}		NH_3 100kPa	
MIL-53(Al)-NH_2	2.3×10^{-9}		*T* = 25 ºC, 95 % RH	H_2O, $-NH_2$, NH_3
	4.1×10^{-8}	0.45	*T* = 80 ºC, 95 % RH	
	1.0×10^{-9}		NH_3 100kPa	
MIL-53(Al)-OH	4.2×10^{-7}		*T* = 25 ºC, 95 % RH	H_2O, −OH, NH_3
	1.9×10^{-6}	0.27	*T* = 80 ºC, 95 % RH	
	4.2×10^{-9}		NH_3 100kPa	
CDMOF-2	4.8×10^{-6}		room temperature, MeOH vapor	−OH, MeOH

The above summary exhibits that MOFs have been the most popular research topic as good proton conductors in related applications, as they are highly porous and easy to functionalize that enable them to provide and accommodate various proton carriers.

In recent years, HOFs have emerged as a new class in the porous crystalline materials regime in which advantages in the ease of their synthesis, structural elucidation via single-crystal X-ray diffraction, low energy consuming regeneration processes, and good thermal stability.[47-49] Hydrogen bonds play a critical role in the construction of such frameworks, and can be utilized to give important functionalities, such as tunable host guest interactions.[50-51] In addition, the H-bonded donor/acceptor groups of building units can serve as proton sources or carriers, while the widespread H-bonds provide diverse proton transportation pathways. Therefore, HOFs can represent a new class of porous materials where the advantage of atomic level insight helps to predict the mechanism of transport phenomenon. Moreover, porosity may allow the incorporation of suitable ion carriers which can result in an ordered arrangement within the confined channels. Thus, rationally choosing such a supramolecular architecture can lead to fabrication of new materials for PEMs. The

features of flexibility and solution processability of HOFs open new possibilities for membrane fabrication, giving light-weight proton conducting solid electrodes.

In 2016, Ghosh et al. reported two bilayer porous HOF-GS-10 and HOF-GS-11,[31] which show high proton conduction under humidified conditions (Figure 1-x). In HOF-GS-10, each disulfonate connects with six adjacent guanidinium cations from two guanidinium–sulfonate sheets by using all its oxygen atoms through charge assisted N–H…O (2.90 to 2.94 Å) interactions, while each guanidinium cation connects with three disulfonates, giving a 2D honeycomblike double-layered network. HOF-GS-11 contains a similar bilayer structure with shifted ribbon H-bonding sheets rather than quasihexagonal sheets. Both HOFs exhibit certain permanent porosity as demonstrated by their CO_2 adsorption isotherms at 195 K. Water sorption studies revealed that HOF-GS-10 shows a water uptake of 3.47 mmol g^{-1}, while that for HOF-GS-11 is up to 11.6 mmol g^{-1}. Given the coherent H-bonding network and porosity, both HOFs are applied to solid-state proton conduction under humid conditions. At 95% RH and 303 K, the proton conductivity of HOF-GS-10 and HOF-GS-11 is up to 0.75×10^{-2} and 1.8×10^{-2} S cm^{-1}, which is comparable to that of MOFs. In addition, HOF-GS-11 also show low activation energy of 0.13 eV compared to PCMOF 5 of 0.16 eV, that further highlighting HOFs as promising lightweight materials for fuel cell technologies.

Also for 2016, Chen and coworkers reported a porphyrin-based porous HOF for the application of proton conduction, which is assembled from 5,10,15,20-tetrakis(4-(2,4-diaminotriazinyl)-phenyl)porphyrin (H2TDPP).[52] In this HOF, (H2TDPP)·6DMF·5THF (HOF-6), each H2TDPP connects with eight adjacent ligands through two types of binding models between DAT–DAT moieties giving a 3D 4,4-connected network of two-fold interpenetrations. This HOF contains 3D intersected pore channels with neutral porphyrins exposed on the pore surface, which can serve as proton donors/acceptors. The solvent accessible void ratio of HOF-6 was estimated to be 63.4%. The BET surface area of desolated HOF-6a was determined to be 130 m^2 g^{-1} based on the CO_2 sorption isotherm at 195 K, confirming its permanent porosity. The

proton conductivity of HOF-6a was examined based on its solid sample. At 97% RH and 300 K, the proton conductivity of HOF-6a is measured to be 3.4×10^{-6} S cm^{-1}, which demonstrates that HOFs are applicable for proton conducting materials.

However, there is still rarely research on proton-conducting HOFs and many aspects in such application have never been involved.

1-5. Crown ethers

As a rapidly developing and highly interdisciplinary emerging discipline, supramolecular chemistry has attracted wide attention from chemists, physicists, materials scientists, and biologists, and is gradually penetrating into many fields including materials chemistry, biochemistry and informatics. Crown ethers were first discovered by Pedersen in 1967,[53] as the structurally simplest and most attractive macrocyclic subjects, have demonstrated fascinating charm in supramolecular host and guest chemistry. At the same time, the emergence of crown ethers also announced the birth of supramolecular chemistry in a certain sense. The discovery of crown ethers was somewhat fortuitous. The scientists of DuPont Company in the United States were preparing (bis(o-epiphenoxy)ethyl) ether, and a very small amount of a white fibrous by-product was isolated. After final isolation and purification and structural analysis, it was finally determined to be a macrocyclic compound, like dibenzo-crown. The complexation properties of such macrocyclic subjects with various metal salts were then thoroughly investigated by Pedersen's complexation studies of metal ions have attracted wide attention from researchers.[54-55] Since then, French scientists and American scientists have done a series of works in the field of cave ethers and spherical ethers, respectively, which have yielded important results.[56-57]

In addition, crown ethers and their derivatives are a general term for a class of macrocyclic compounds that contain multiple oxygen atoms. The common crown ethers and their derivatives include crown, dibenzo-crown, tribenzo-crown as well as cave acids and various substituted crown ethers derived from the above-mentioned

crown ethers. Early studies on crown ethers focused on the coordination interaction between crown ethers and metal cations. The host crown acid molecule and the guest metal ion form a host-guest complex with certain stability and three-dimensional structure through dipole ion interaction.[59-61] For example, alkali metal salts can be dissolved in a solution of benzene containing a small amount of dibenzo-crown to form a solution commonly called violet benzene, which is due to the entry of potassium ions into the cavity of the crown acid containing oxygen atoms, forming a crown-like host-guest complex. And scientists have also used the coordination of crown acid with, and other metal ions to successfully introduce the template effect in the chemical synthesis of crown ethers, which can obtain higher yields, laying a solid foundation for the derivatization and functionalization of crown ethers. With the further research, scientists also found that the subject crown ether molecule can form a variety of complexes by coordination with press ions, organic neutral molecules or anions. Unlike the coordination of metal cations, crown ethers form more stable host-guest complexes mainly through hydrogen bonding, electrostatic interaction, dipole interaction and charge transfer.

1-6. Survey of this thesis

It is well known that crown ethers with numerous advantages such as high-selective recognition have been the most attractive macrocyclic groups in supermolecule chemistry. However, there is very few reports of MOFs and COFs composed of crown ethers, especially, there is no example of crown ether-based HOFs. Probably, the high flexibility and various low-symmetric conformations of the crown ether moiety make it a big challenge to construct such HOFs. On the other hands, theoretical calculation indicated B18C6 with H_3O^+ cations located in the cavities of crown ether interact with water molecules,[62] revealed the formation of H-bonded networks which enable proton transfer though channels. However, the organic

electrolyte materials based on crown ethers are hitherto unknown. Herein, it is expected to construct a series of proton conductive porous crystalline HOFs based on crown ethers.

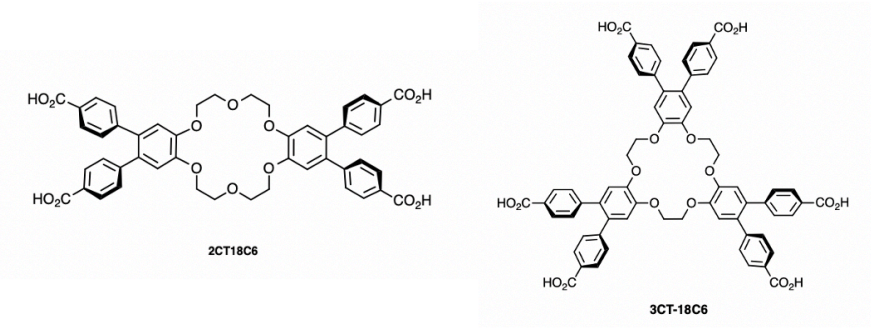

Figure 1-3. Building block molecules of 2CT-18-6 and 3CT-18C6.

The author's hypothesis is as follows (Figure 1-3): (1) The carboxyl group with the highly directional nature is appropriate to construct HOFs. (2) The building block molecule can form different porous motifs for permanent porosity. (3) The 18C6 ethers has the extraordinary features in binding inorganic or organic guests for multifunctionality.

1-7. References

1. K. D. Kreuer, *Chem. Mater.*, **1996**, 8, 610–641.
2. K. D. Kreuer, S. J. Paddison, E. Spohr and M. Schuster, *Chem. Rev.*, **2004**, 104, 4637–4678.
3. L. C. Malavasi, A. J. Fisherb and M. S. Islam, *Chem. Soc. Rev.*, **2010**, 39, 4370–4387.
4. S. S. Ivanchev, *Russ. J. Appl. Chem.*, **2008**, 81, 569–584.
5. S. M. Haile, D. A. Boysen, C. R. I. Chisholm and R. B. Merle, *Nature*, **2001**, 410, 910–913.
6. D. Hoel and E. Grunwald, *J. Phys. Chem.*, **1977**, 81, 2135–2136.
7. G. Alberti and M. Casciola, *Solid State Ionics*, **2001**, 145, 3–16.
8. J. Otomo, N. Minagawa, C. J. Wen, K. Eguchi and H. Takahashi, *Solid State. Ionics*, **2003**, 156, 357–369.
9. V. G. Ponomareva and E. S. Shutova, *Solid State Ionics*, **2007**, 178, 729–734.
10. J. A. Asensio, E. M. SaÅLncheza and P. GoÅLmez-Romero, *Chem. Soc. Rev.*, **2010**, 39, 3210–3239.
11. K. D. Kreuer, A. Fuchs, M. Ise, M. Spaeth and J. Maier, *Electrochim. Acta.*, **1998**, 43, 1281–1288.
12. M. Casciola, S. Chieli, U. Costantino and A. Peraio, *Solid State Ionics*, **1991**, 46, 53–59.
13. O. Nakamura, T. Kodama, I. Ogino and Y. Miyake, *Chem. Lett.*, **1979**, 17–18.
14. M. L. Wei, X. X. Wang and X. Y. Duan, *Chem. – Eur. J.*, **2013**, 19, 1607–1616.
15. J. Miao, Y. Liu, Q. Tang, D. He, G. Yang, Z. Shi, S. Liu and Q. Wu, *Dalton. Trans.*, **2014**, 43, 14749–14755.
16. Y. Liu, X. Yang, J. Miao, Q. Tang, S. Liu, Z. Shi and S. Liu, *Chem. Commun.*, **2014**, 50, 10023–10026.
17. J. Li, X. L. Cao, S. L. Li, Z. M. Su and Y. Q. Lan, *Chem. – Eur. J.*, **2016**, 22, 9299–9304.

18. P. Ramaswamy, N. E. Wong and G. K. H. Shimizu, *Chem. Soc. Rev.*, **2014**, 43, 5913–5932.
19. M. Yoon, K. Suh, S. Natarajan and K. Kim, *Angew. Chem., Int. Ed.*, **2013**, 52, 2688–2700.
20. T. Yamada, K. Otsubo, R. Makiurac and H. Kitagawa, *Chem. Soc. Rev.*, **2013**, 42, 6655–6669.
21. S. Chandra, T. Kundu, S. Kandambeth, R. BabaRao, Y. Marathe, S. M. Kunjir and R. Banerjee, *J. Am. Chem. Soc.*, **2014**, 136, 6570–6573.
22. K. D. Kreuer, *Chem. Mater.*, **1996**, 8, 610–641.
23. P. Ramaswamy, N. E. Wong and G. K. H. Shimizu, *Chem. Soc. Rev.*, **2014**, 43, 5913–5932.
24. N. Agmon, *Chem. Phys. Lett.*, **1995**, 244, 456–462.
25. S. Kanda, K. Yamashita, K. Ohkawa, Bull. *Chem. Soc. Jpn.*, **1979**, 52, 3296−3301.
26. Y. Nagao, M. Fujishima, R. Ikeda, S. Kanda, H. Kitagawa, *Synth. Met.*, **2003**, 133−134, 431−432.
27. Y. Nagao, T. Kubo, K. Nakasuji, R. Ikeda, T. Kojima, H. Kitagawa, *Synth. Met.*, **2005**, 154, 89−92.
28. M. Sadakiyo, T. Yamada, H. Kitagawa, J. Am. Chem. Soc., **2009**, 131, 9906−9907.
29. Y. S. Wei, X. P. Hu, Z. Han, X. Y. Dong, S. Q. Zang, T. C. W. Mak, *J. Am. Chem. Soc.*, **2017**, 139, 3505−3512.
30. N. T. T. Nguyen, H. Furukawa, F. Gándara, C. A. Trickett, H. M. Jeong, K. E. Cordova, O. M. Yaghi, *J. Am. Chem. Soc.*, **2015**, 137, 15394−15397.
31. S. S. Nagarkar, S. M. Unni, A. Sharma, S. Kurungot, S. K. Ghosh, *Angew. Chem., Int. Ed.*, **2014**, 53, 2638−2642.
32. D. -W. Lim and H. Kitagawa, *Chem. Rev.*, **2020**, 120, 8416−8467.
33. Y. S. Wei, X. P. Hu, Z.Han, T. C. W. Mak, *J. Am. Chem. Soc.*, **2017**, 139, 3505−3512.

34. N. T. T. Nguyen, H. Furukawa, F. Gándara, C. A. Trickett, H. M. Jeong, K. E. Cordova, O. M. Yaghi, *J. Am. Chem. Soc.*, **2015**, 137, 15394−15397.
35. S. S. Nagarkar, S. M. Unni, A. Sharma, S. Kurungot, S.K. Ghosh, *Angew. Chem., Int. Ed.*, **2014**, 53, 2638−2642.
36. A. Shigematsu, T. Yamada, H. Kitagawa, *J. Am. Chem. Soc.*, **2011**, 133, 2034−2036.
37. P. Rought, C. Marsh, S. Pili, I. P. Silverwood, V. G. Sakai, M. Li, Whitehead, G. et. al., *Chem. Sci.*, **2019**, 10, 1492−1499.
38. W. J. Phang, W. R. Lee, K. Yoo, D. W. Ryu, B. Kim, C. S. Hong, *Angew. Chem., Int. Ed.*, **2014**, 53, 8383−8387.
39. F. Yang, G. Xu, Y. Dou, W. Zhou, J. R. Li, B. Chen, *Nat. Energy*, **2017**, 2, 877−883.
40. N. C. Jeong, B. Samanta, C. Y. Lee, J. T. Hupp, *J. Am. Chem. Soc.*, **2012**, 134, 51−54.
41. F. M. Zhang, L. Z. Dong, J. S. Qin, W. Guan, J. Liu, S. L. Li, H. C. Zhou, *J. Am. Chem. Soc.*, **2017**, 139, 6183−6189.
42. D. Umeyama, S. Horike,M. Inukai, Y. Hijikata, S. Kitagawa, *Angew. Chem., Int. Ed.*, **2011**, 50, 11706−11709.
43. J. Lee, D.-W. Lim, S. Dekura, H. Kitagawa, *ACS Appl. Mater. Interfaces*, **2019**, 11, 12639−12646.
44. J. M. Taylor, S. Dekura, R. Ikeda, H. Kitagawa, *Chem. Mater.*, **2015**, 27, 2286−2289.
45. J. M. Taylor, T. Komatsu, S. Dekura, K. Otsubo, M. Takata, H.Kitagawa, *J. Am. Chem. Soc.*, **2015**, 137, 11498−11506.
46. M. Inukai, S. Horike, S. Nagarkar, Y. Nishiyama, M. Malon et. al, A. Hayashi, *J. Am. Chem. Soc.*, **2016**, 138, 8505−8511.
47. Y. He, S. Xiang, B. Chen, *J. Am. Chem. Soc.*, **2011**, 133, 14570–14573.
48. X. Z. Luo, X. J. Jia, J. H. Deng, J. L. Zhong, H. J. Liu, K. J. Wang, D. C. Zhong, *J. Am. Chem. Soc.*, **2013**, 135, 11684–11687;

49. C. A. Zentner, H. W. H. Lai, J. T. Greenfield, R. A. Wiscons, M. Zeller, C. F. Campana, O. Talu, S. A. FitzGeralde, J. L. C. Rowsell, *Chem. Commun.*, **2015**, 51, 11642–11645.
50. R. Custelcean, M. D. Ward, *Cryst. Growth Des.*, **2005**, 5, 2277–2287;
51. P. Li, H. D. Arman, H. Wang, L. Weng, K. Alfooty, R. F. Angawi, B. Chen, *Cryst. Growth Des.*, **2015**, 15, 1871–1875.
52. W. Yang, F. Yang, T.-L. Hu, S. C. King, H. Wang, H. Wu, W. Zhou, J.-R. Li, H. D. Arman and B. Chen, *Cryst. Growth Des.*, **2016**, 16, 5831–5835.
53. C. J. Pedersen, *J. Am. Chem. Soc.*, **1967**, 89, 7017.
54. H. E. Simmons and C. H. Park, *J. Am. Chem. Soc.*, **1968**, 90, 2428–2429.
55. C. H. Park and H. E. Simmons, *J. Am. Chem. Soc.*, **1968**, 90, 2429–2432.
56. B. Dietrich, J. M. Lehn and J. P. Sauvage, Tetrahedron Lett., **1969**, 10, 2885–2892.
57. D. J. Cram, *Science*, **1983**, 219, 1177–1183.
58. D. J. Cram, *Angew. Chem., Int. Ed. Engl.*, **1986**, 25, 1039–1057.
59. D. J. Cram, *Angew. Chem., Int. Ed. Engl.*, **1988**, 27, 1009–1020.
60. W. Saenger, J. Jacob, K. Gessler, T. Steiner, D. Hoffmann, H. Sanbe, K. Koizumi, S. M. Smith and T. Takaha, *Chem. Rev.*, **1998**, 98, 1787–1802.
61. I. Tabushi, Y. Kuroda and A. Mochizuki, *J. Am. Chem. Soc.*, **1980**, 102, 1152–1153.
62. G. Crini, *Chem. Rev.*, **2014**, 114, 10940–10975.
63. M. Bühl, G. Wipff, *J. Am. Chem. Soc.*, **2002**, 124, 4473−4480.

Chapter 2

Synthesis the Surveyed Synthon by 18-Crown-6 Ethers with Dicarboxy-*o*-terphenyl groups

2-1. Introduction

In Chapter 2, the author systematically introduces the synthetic routes of all compounds, including **1CT-18C6**, **2CT-18C6**, **2CT-24C8** and **3CT-18C6**. Additionally, the NMR spectrums indicate the good purity of each compound, which are critical for the further studies.

All the chemicals used as starting materials, reagents and solvents were purchased from commercial suppliers and used as received without further purification. Analytical thin layer chromatography (TLC) was carried out on aluminum sheets coated with silica gel (Kieselgel 60F254, Merck). Column chromatographic purifications were performed using silica gel (63-200 μm, Merck and 64-210 μm, Wakosil.). Unless stated otherwise, reported yields refer to analytically pure samples.

2-2. Synthesis of 1CT-18C6.

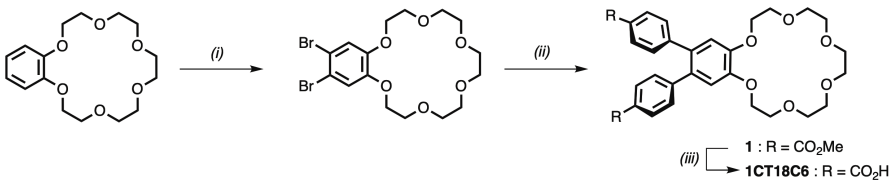

Scheme 2-1. Synthesis of **4, 5-Dibenzoic acid benzo-18-crown-6 (1CT-18C6).***

* Reagents and conditions: (i) (a) Bromine, acetic acid, 2 h, (b) 65 ºC, 12 h, 81%.[1] (ii) (a) $Pd(PPh_3)_4$, K_2CO_3, dry THF, 15 min, (b) 4-methoxycarbonylphenyl boronic acid, MeOH, 70 ºC, 48 h, 72%; (iii) (a) 10% $NaOH_{aq}$, THF, 60 ºC, 48 h, (b) HCl, 77%.

4,5-Dibromodibenzo-18-crown-6. Benzo[18]crown-6 ether (2.00 g, 6.40 mmol) was dissolved in acetic acid (80 mL). Bromine (5.00 g, 31.3 mmol) was added to the solution, and the mixture was stirred for 12 h at 85 ˚C. After cooling the solution, the

orange powder was filtered and washed with water, $Na_2S_2O_3$(aq), MeOH (two times for each) to give white residue (2.43 g, 81%).

^{1}H NMR (400 MHz, $CDCl_3$): δ 7.07 (s, 2H), 4.12 (d, *J* = 5.7 Hz, 4H), 3.92 (d, *J* = 5.6 Hz, 4H), 3.77 (d, *J* = 6.0 Hz, 4H), 3.76-3.64 (m, 8H) ppm (Figure 2-1); ^{13}C NMR: (100 MHz, $CDCl_3$): δ 148.56, 118.17, 115.37, 70.93, 70.74, 70.69, 69.40, 69.24 ppm. (Figure 2-2)

4,5-Dibenzoic ester benzo-18-crown-6 (1). 4,5-dibromobenzo-18-crown-6 (0.805 g, 1.72 mmol), K_2CO_3 (0.711 g, 5.11 mmol) and $Pd(PPh_3)_4$ (0.13 g, 0.112 mmol) were dissolved in THF (100 mL) and stirred for 15 min. 4-methoxycarbonylphenyl boronic acid (0.927 g, 5.1 mmol), dissolved in methanol (30 mL), was added to the solution and stirred for 48 h under reflux condition. After being cooled to the room temperature, the mixture was concentrated in a rotary evaporator, extracted with chloroform, washed with water and dried over anhydrous $MgSO_4$. The product was purified with column chromatography (silica gel, chloroform) to give **1** (0.713 g, 72%) as a white solid.

^{1}H NMR (400 MHz, $CDCl_3$): δ 7.84 (d, 4H), 7.13 (d, 4H), 6.93 (s, 2H), 4.27-4.20 (m, 8H), 3.98-3.89 (m, 4H), 3.88 (s, 6H), 3.82-3.66 (m, 12H) ppm (Figure 2-3); ^{13}C NMR: (100 MHz, $CDCl_3$): δ 166.99, 148.60, 145.84, 132.58, 129.99, 129.41, 128.24, 115.60, 69.91, 69.10, 52.15 ppm (Figure 2-4).

4, 5-Dibenzoic acid benzo-18-crown-6 (1CT-18C6). To a solution of **1** (0.707 g, 1.21 mmol) dissolved in THF (20 mL) was added 10% $NaOH_{aq}$ (10 mL). After stirred at 65 ºC for 48 h, 6 M HCl aqueous solution was added to the organic layer until it became neutral. The product was collected by centrifugation and washed with water for three time. **1CT-18C6** was obtained in vacuo as a white solid (0.512 g, 77 %).

^{1}H NMR(400 MHz, DMSO): δ 7.74 (d, *J* = 7.9 Hz, 4H), 7.17 (d, *J* = 7.9 Hz, 4H), 7.00 (s, 2H), 4.21-4.14 (m, 4H), 3.75 (d, *J* = 5.9 Hz, 4H) , 3.60-3.56 (m, 4H) , 3.53 (d, *J* = 5.9 Hz, 4H) , 3.50 (s, 4H) ppm (Figure 2-5); ^{13}C NMR: (100 MHz, DMSO-d_6) δ 167.7,

148.4, 145.7, 132.0, 130.5, 129.6, 129.4, 115.3, 70.29, 70.25, 69.1, 68.6 ppm (Figure 2-6); ESI-MS *m/z* calc. for $[M]^+$ $C_{30}H_{32}O_{10}$: 552.19; found: 552.20.

2-3. Synthesis of 2CT-18C6.

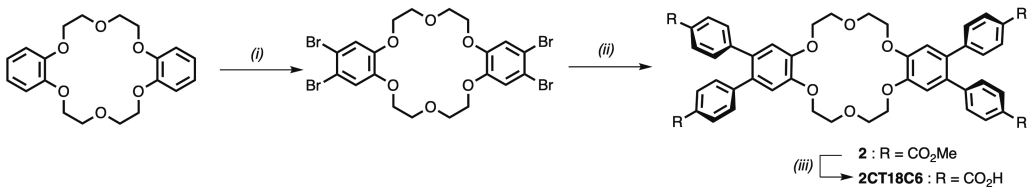

Scheme 2-2. Synthesis of **4,4',5,5'-Terabenzoic acid dibenzo-18-crown-6 (2CT-18C6)**.*

* Reagents and conditions: (i) (a) Bromine, acetic acid, 2 h, (b) 65 ºC, 12 h, 86%.[1] (ii) (a) $Pd(PPh_3)_4$, K_2CO_3, dry THF, 15 min, (b) 4-methoxycarbonylphenyl boronic acid, MeOH, 70 ºC, 48 h, 76%; (iii) (a) 10% $NaOH_{aq}$, THF, 60 ºC, 48 h, (b) HCl, 73%.

4,4',5,5'-Tetrabromodibenzo-18-crown-6. Dibenzo[18]crown-6 ether (1.61 g, 4.47 mmol) was dissolved in acetic acid (50 mL). Bromine (5.00 g, 31.3 mmol) was added to the solution, and the mixture was stirred for 12 h at 85 ˚C. After cooling the solution, the orange powder was filtered and washed with water, $Na_2S_2O_3$(aq), MeOH (two times for each) to give white residue (2.61 g, 86%).^{1}H NMR (400 MHz, $CDCl_3$): 7.03 (s, 4H), 4.08 (s, 8H), 3.96 (s, 8H) ppm (Figure 2-7); ^{13}C NMR (100 MHz, $CDCl_3$): δ 148.67, 117.95, 115.21, 69.72, 69.08 ppm (Figure 2-8).

4,4',5,5'-Terabenzoic ester dibenzo-18-crown-6 (2). 4,4',5,5'-tetrabromodibenzo-18-crown-6 (4.05 g, 5.99 mmol), K_2CO_3 (4.16 g, 30.1 mmol) and $Pd(PPh_3)_4$ (0.477 g, 0.413 mmol) were dissolved in THF (100 mL) and stirred for 15 min. 4-methoxycarbonylphenyl boronic acid (5.39 g, 30.0 mmol), dissolved in methanol (50 mL), was added to the solution and stirred for 48 h under reflux condition. After being cooled to the room temperature, the mixture was concentrated in a rotary evaporator, extracted with chloroform, washed with water and dried over anhydrous $MgSO_4$. The

product was purified with column chromatography (silica gel, chloroform) to give **2** (4.11 g, 76%) as a white solid.

^{1}H NMR (400 MHz, $CDCl_3$): δ 7.85 (d, J = 8.4 Hz, 8H), 7.13 (d, J = 8.4 Hz, 8H), 6.94 (s, 4H), 4.26 (t, J = 4.5 Hz, 8H), 4.07 (t, J = 4.6 Hz, 8H), 3.88 (s, 12H) ppm (Figure 2-9); ^{13}C NMR: (100 MHz, $CDCl_3$) δ 167.02, 148.71, 145.82, 132.71, 130.00, 129.44, 128.27, 115.97, 70.03, 69.31, 52.19 ppm (Figure 2-10).

4,4',5,5'-Terabenzoic acid dibenzo-18-crown-6 (2CT-18C6). To a solution of **2** (1.07 g, 1.19 mmol) dissolved in THF (30 mL) was added 10 % $NaOH_{aq}$ (10 mL). After stirred at 60 ºC for 48 h, 6 M HCl aqueous solution was added to the organic layer until it became neutral. The product was collected by centrifugation and washed with water for three time. **2CT-18C6** was obtained in vacuo as a white solid (0.738 g, 73 %).

^{1}H NMR (400 MHz, DMSO-d_6): δ 7.75 (d, J = 7.9 Hz, 8H), 7.19 (d, J = 7.9 Hz, 8H), 7.00 (s, 4H), 4.22-4.19 (m, 8H), 3.89-3.85 (m, 8H) ppm (Figure 2-11); ^{13}C NMR: (100 MHz, DMSO-d_6) δ 167.67, 147.93, 145.76, 131.89, 130.52, 129.60, 129.23, 114.43, 69.13, 68.09 ppm (Figure 2-12); ESI-MS *m/z* calc. for $[M+Na]^+$ $C_{48}H_{40}O_{14}$: 840.22; found: 840.24.

2-4. Synthesis of 2CT-24C8.

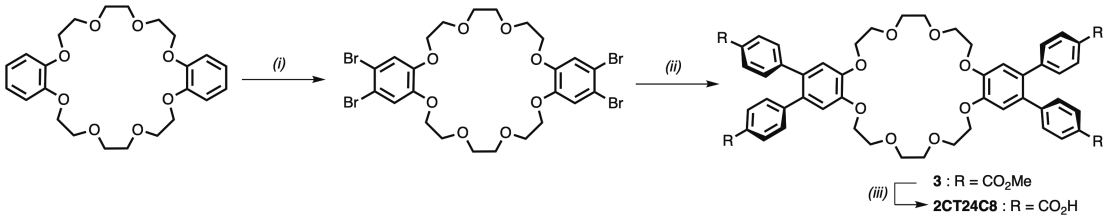

Scheme 2-3. Synthesis of **4,4',5,5'-erabenzoic acid dibenzo-24-crown-8** (**2CT-24C8**).*

* Reagents and conditions: (i) (a) Bromine, acetic acid, 2 h, (b) 65 ºC, 12 h, 88%.[1] (ii) (a) $Pd(PPh_3)_4$, K_2CO_3, dry THF, 15 min, (b) 4-methoxycarbonylphenyl boronic acid, MeOH, 70 ºC, 48 h, 72%; (iii) (a) 10% KOH_{aq}, THF, 60 ºC, 48 h, (b) HCl, 75%.

4,4',5,5'-Tetrabromodibenzo-24-crown-8. Dibenzo[24]crown-8 ether (2.00 g, 4.46 mmol) was dissolved in acetic acid (50 mL). Bromine (5.00 g, 31.3 mmol) was added to the solution, and the mixture was stirred for 12 h at 85 ˚C. After cooling the solution, the orange powder was filtered and washed with water, $Na_2S_2O_3$(aq), MeOH (two times for each) to give white residue (2.99 g, 88%).
^{1}H NMR (400 MHz, $CDCl_3$): 7.03 (s, 4H), 4.08 (s, 8H), 3.96 (s, 8H) ppm (Figure 2-13); ^{13}C NMR (100 MHz, $CDCl_3$): δ 148.67, 117.95, 115.21, 69.72, 69.08 ppm (Figure 2-14).

4,4',5,5'-Terabenzoic ester dibenzo-24-crown-8 (3). 4,4',5,5'-tetrabromodibenzo-24-crown-8 (5.00 g, 6.54 mmol), K_2CO_3 (4.52 g, 32.7 mmol) and $Pd(PPh_3)_4$ (0.522 g, 0.440 mmol) were dissolved in THF (100 mL) and stirred for 15 min. 4-methoxycarbonylphenyl boronic acid (5.87 g, 32.7 mmol), dissolved in methanol (50 mL), was added to the solution and stirred for 48 h under reflux condition. After being cooled to the room temperature, the mixture was concentrated in a rotary evaporator, extracted with chloroform, washed with water and dried over anhydrous $MgSO_4$. The product was purified with column chromatography (silica gel, chloroform) to give **2** (4.64 g, 72%) as a white solid. ^{1}H NMR (400 MHz, $CDCl_3$): δ 7.85 (d, J = 7.6 Hz, 8H), 7.13 (d, J = 7.6 Hz, 8H), 6.94 (s, 4H), 4.27-4.23 (m, 8H), 4.09-4.02 (m, 8H), 3.88 (s, 12H) ppm (Figure 2-15); ^{13}C NMR: (100 MHz, $CDCl_3$) δ 167.02, 148.71, 145.82, 132.71, 130.00, 129.44, 128.27, 115.97, 70.03, 69.31, 52.19 ppm (Figure 2-16).

4,4',5,5'-Terabenzoic acid dibenzo-24-crown-8 (2CT-24C8). To a solution of **3** (1.51 g, 1.53 mmol) dissolved in THF (30 mL) was added 10 % KOH_{aq} (10 mL). After stirred

at 60 ºC for 48 h, 6 M HCl aqueous solution was added to the organic layer until it became neutral. The product was collected by centrifugation and washed with water for three time. **2CT-24C8** was obtained in vacuo as a white solid (1.08 g, 75 %).

^{1}H NMR (400 MHz, DMSO-d_6): δ 7.75 (d, J = 7.9 Hz, 8H), 7.19 (d, J = 7.9 Hz, 8H), 7.00 (s, 4H), 4.19 (s, 8H), 3.85 (s, 8H) ppm (Figure 2-17); ^{13}C NMR: (100 MHz, DMSO-d_6) δ 167.67, 147.93, 145.76, 131.89, 130.52, 129.60, 129.23, 114.43, 69.13, 68.09 ppm (Figure 2-18).

2-5. Synthesis of 3CT-18C6.

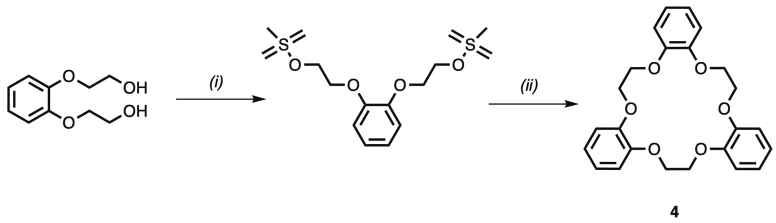

Scheme 2-4. Synthesis of **2,3,8,9,14,15-hexahydrotribenzo-18-crown-6** (**4**).*

* Reagents and conditions: (i) (a) Et_3N, methanesulfonyl chloride, CH_2Cl_2, 0 ºC, 2 h, (b) HCl, H_2O, 15 min, rt, 85%.[2] (ii) (a) bisphenol, Cs_2CO_3, dry MeCN, 70 ºC, 4 h, (b) dimesylate, MeCN, 18 h, 85%.[3]

2,2'-[1,2-Phenylenebis(oxy)]diethanol.[2] Pyrocatechol (16.5 g, 0.151 mol) and 2-chloroethanol (30 mL) were added consecutive to a solution of NaOH (14.4 g, 0.362 mol) in H_2O (300 mL) and the resulting mixture was stirred at 70 ºC during 20 h. It was cooled, second portions of 2-chloroethanol (15 mL) and NaOH (9.05 g, 0.283 mol) were added consecutively, and the resulting mixture was stirred at 70 ºC for further 48 h to give a plentiful suspension. On cooling to room temperature, it was extracted with CH_2Cl_2 at least 6 times with 100 mL each time. Then combined extracted were washed with H_2O, dried over anhydrous Na_2SO_4 and concentrated in vacuum resulting in the formation of viscous cherry liquid. It was diluted with Et_2O, precipitate was collected, washed with Et_2O for several times and dried on the air to give **2,2'-[1,2-Phenylenebis(oxy)]diethanol** (28.1 g, 95%) as light-beige powder.

^{1}H NMR (400 MHz, $CDCl_3$): δ 6.91 (p, J = 2.5 Hz, 4H), 4.15 (s, 2H), 4.13-4.00 (m, 4H), 3.93-3.87 (m, 4H).

1, 2-Bis(2'-hydroxyethoxy)benzene Dimesylate. The **2,2'-[1,2-Phenylenebis(oxy)]diethanol** (5.00 g, 25.3 mmol) was dissolved in CH_2Cl_2 (100 mL) and cooled to 0 ºC under a nitrogen atmosphere. Triethylamine (9.2 mL) was diluted

with CH_2Cl_2 (25 mL) and added to the solution of the diol. To the stirred solution, a solution of methanesulfonyl chloride (4.3 mL) in CH_2Cl_2 (25 mL) was added to the reaction mixture at 0 ºC, dropwise via an addition funnel. After completion of the addition, the reaction mixture was allowed to warm to room temperature over 2h. A 5% aq HCl solution was added, and the mixture was stirred for 15 min. The biphasic mixture was decanted into a separatory funnel and the organic layer was separated. The organic solution was washed with saturated aq. $NaHCO_3$, distilled H_2O and brine. The solution was dried over $MgSO_4$ and the solvent was removed in vacuo. Solid products of **Dimesylate** (7.45 g, 85%) were recrystallized from MeOH.

^1H NMR (400 MHz, $CDCl_3$): δ 6.97-6.94 (m, 4H), 4.62-4.57 (m, 4H), 4.30-4.25 (m, 4H), 3.12 (s, 6H).

2,3,8,9,14,15-hexahydrotribenzo-18-crown-6 (4). MeCN was placed in a three-necked flask ultrasound for 30 min under N_2. The bisphenol (1.00 g, 4.06 mmol) was added, and the solution was purged for an additional 20 min, then Cs_2CO_3 (3.31g, 10.2 mmol) was added. The heterogeneous mixture was stirred at 70 ºC under nitrogen for 4 h. A solution of the dimesylate (1.44g, 4.06 mmol) in MeCN (40 mL) was added to the mixture by the pressure titration funnel overnight. The reaction mixture was continued to stir for 18 h after the addition was finished. The mixture was cooled to room temperature and filtered. The residue was rinsed with CH_2Cl_2. The combined solution was evaporated and dissolved in CH_2Cl_2. The organic solution was washed with HCl, then H_2O and brine for three times as well dried over $MgSO_4$ and evaporate to give **4** (1.41g, 85 %) as a white solid.

^1H NMR (400 MHz, $CDCl_3$): δ 6.91 (s, 12H), 4.39 (s, 12H) ppm (Figure 2-19). ^{13}C NMR: (100 MHz, $CDCl_3$) δ 148.99, 121.87, 115.35, 67.92 ppm (Figure 2-20).

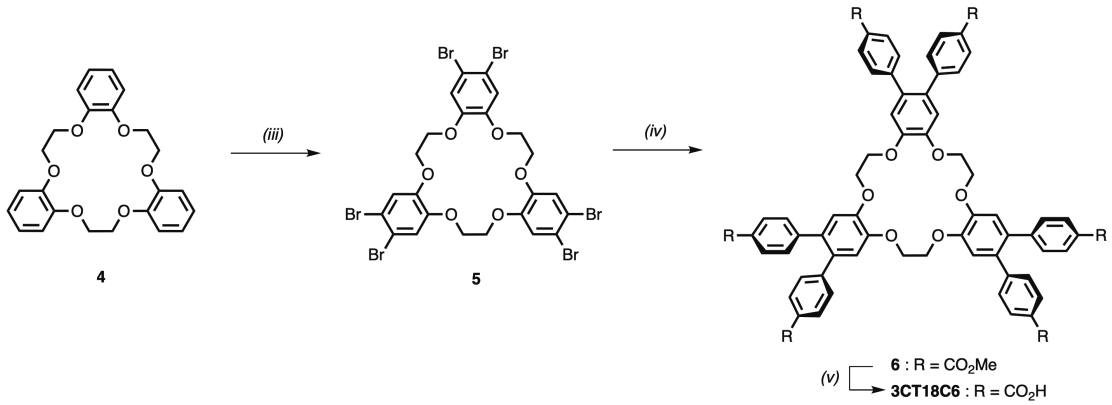

Scheme 2-5. Synthesis of **2,3,8,9,14,15-hexabenzoic acid tribenzo-18-crown-6** (**3CT-18C6**).*

* Reagents and conditions: (iii) (a) Bromine, acetic acid, 2 h, (b) 65 ºC, 12 h, 84%.[1] (iv) (a) $Pd(PPh_3)_4$, K_2CO_3, dry THF, 15 min, (b) 4-methoxycarbonylphenyl boronic acid, MeOH, 70 ºC, 72 h, 73%; (v) (a) 10% $NaOH_{aq}$, THF, 60 ºC, 72 h, (b) HCl, 70%.

2,3,8,9,14,15-hexabromotribenzo-18-crown-6 (5). A stirred suspension of **4** (1.31 g, 3.18 mmol) in acetic acid was added bromine (5.00 g). After 2 h dark orange solution was obtained and refluxed for 12 h until a white solid gave below a orange solution. The solid was filtered and washed with acetic acid then acetone to give **5** (2.37 g, 84 %) as a white solid.

^{1}H NMR (400 MHz, $CDCl_3$): δ 7.10 (s, 6H), 4.32 (s, 12H) ppm (Figure 2-21); ^{13}C NMR: (100 MHz, $CDCl_3$) δ 148.36, 119.03, 115.77, 67.51 ppm (Figure 2-22); ESI-MS *m/z* calc. for $[M+Na]^+$ $C_{24}H_{18}Br_6O_6Na$: 904.6037; found: 904.61.

2,3,8,9,14,15-hexabenzoic ester tribenzo-18-crown-6 (6). A mixture of **5** (2.37g, 2.69 mmol), K_2CO_3 (2.26 g, 16.4 mmol) and $Pd(PPh_3)_4$ (0.22 g, 0.19 mmol) in THF was stirred for 15 min. 4-methoxycarbonylphenyl boronic acid (3.43 g, 19.1 mmol), dissolved in methanol (35 mL), was added to the solution under reflux condition for 3 days. The reaction mixture was concentrated in vacuo, extracted by chloroform, washed with water, and dry over anhydrous $MgSO_4$. The product was purified with column

chromatography (silica gel, chloroform) and HPLC to give **6** (2.41 g, 73 %) as a white solid.

^{1}H NMR (400 MHz, $CDCl_3$): δ 7.85 (d, *J* = 8.4 Hz, 12H), 7.12 (d, *J* = 8.4 Hz, 12H), 7.00 (s, 6H), 4.53 (s, 12H), 3.88 (s, 18H) ppm (Figure 2-23). ^{13}C NMR: (100 MHz, $CDCl_3$) δ 166.96, 148.47, 145.54, 133.17, 129.94, 129.49, 128.42, 117.00, 67.93, 52.21 ppm (Figure 2-24); ESI-MS *m/z* calc. for $[M+Na]^+$ $C_{72}H_{60}O_{18}Na$: 1235.37; found: 1235.38.

2,3,8,9,14,15-hexabenzoic acid tribenzo-18-crown-6 (3CT-18C6). To a solution of **3** (2.12 g, 1.75 mmol) dissolved in THF (100 ml) was added 10% $NaOH_{aq}$ (30 ml). After stirred at 60 ºC for 3 days, 12 M HCl aqueous solution was added to the organic layer until it became neutral. The product was collected by centrifugation and washed with water for three time. **3CT-18C6** was obtained in vacuo as a white solid (1.32 g, 70 %). ^{1}H NMR (400 MHz, CD_3OD): δ 7.75 (d, *J* = 8.0 Hz, 12H), 7.19 (d, *J* = 8.0 Hz, 18 H), 4.52 (s, 12H) ppm (Figure 2-25); ^{13}C NMR: (100 MHz, CD_3OD) δ 167.71, 147.76, 145.63, 132.12, 130.51, 129.57, 126.93, 115.15, 66.61 ppm (Figure 2-26); ESI-MS *m/z* calc. for $[M-H]^+$ $C_{66}H_{47}O_{18}$: 1127.28; found: 1127.28.

2-6. ^{1}H and ^{13}C NMR Spectra.

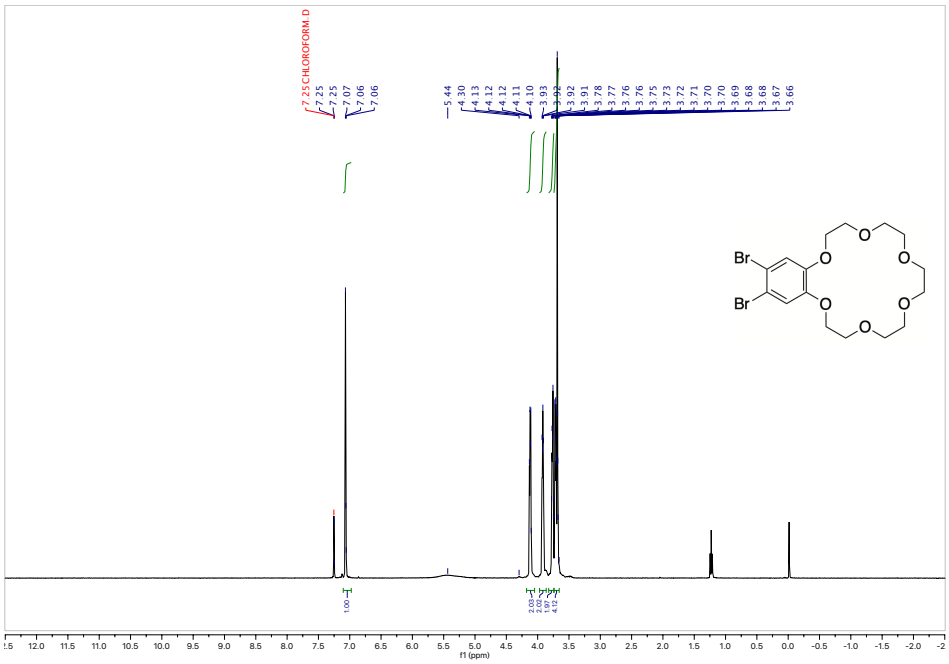

Figure 2-1. ^{1}H NMR (400 MHz, $CDCl_3$) spectrum of **4,5-Dibromodibenzo-18-crown-6**.

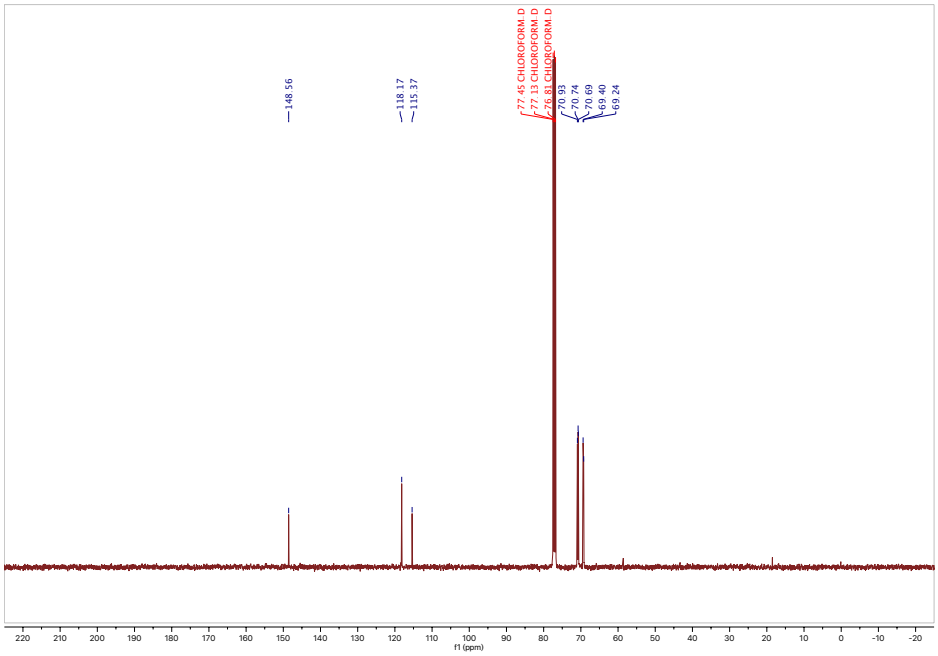

Figure 2-2. ^{13}C NMR (100 MHz, $CDCl_3$) spectrum of **4,5-Dibromodibenzo-18-crown-6v**.

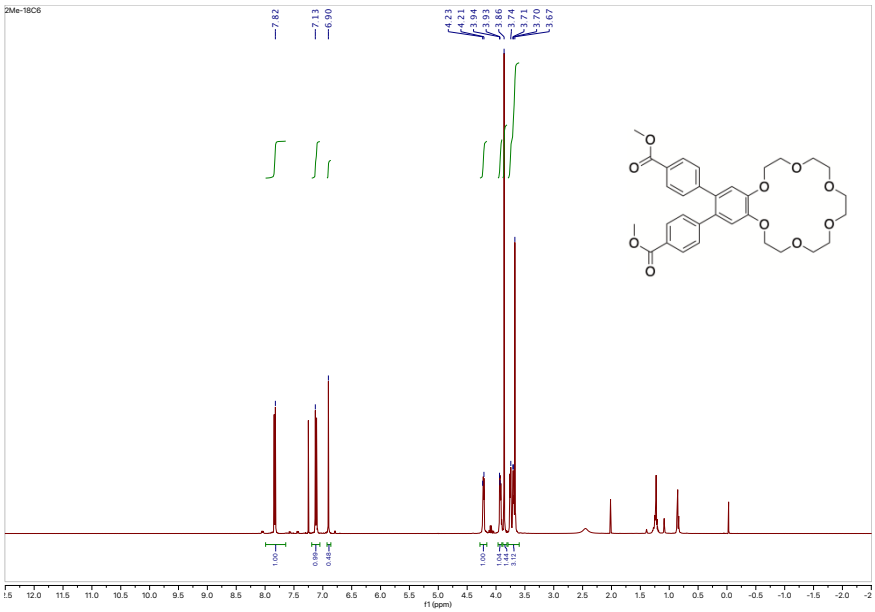

Figure 2-3. ^{1}H NMR (400 MHz, $CDCl_3$) spectrum of **1**.

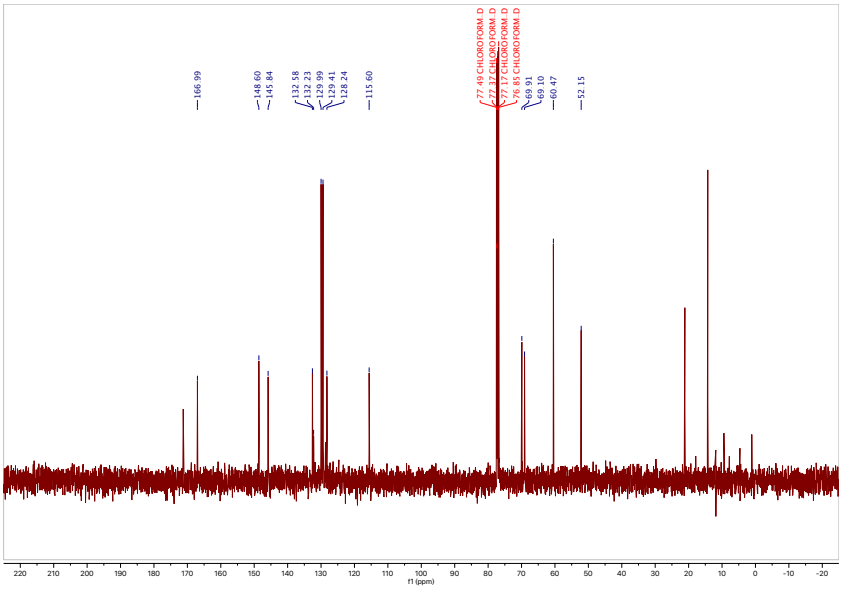

Figure 2-4. ^{13}C NMR (100 MHz, $CDCl_3$) spectrum of **1**.

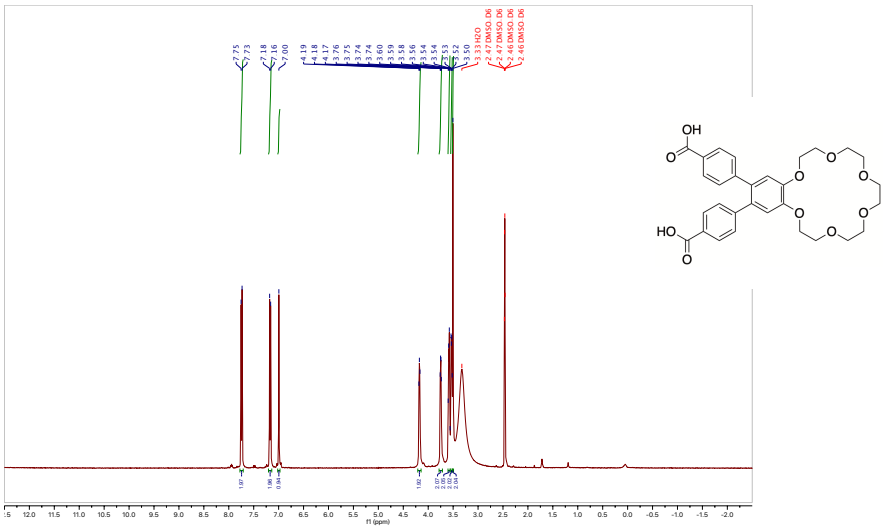

Figure 2-5. ^{1}H NMR (400 MHz, DMSO-d_6) spectrum of **1CT-18C6**.

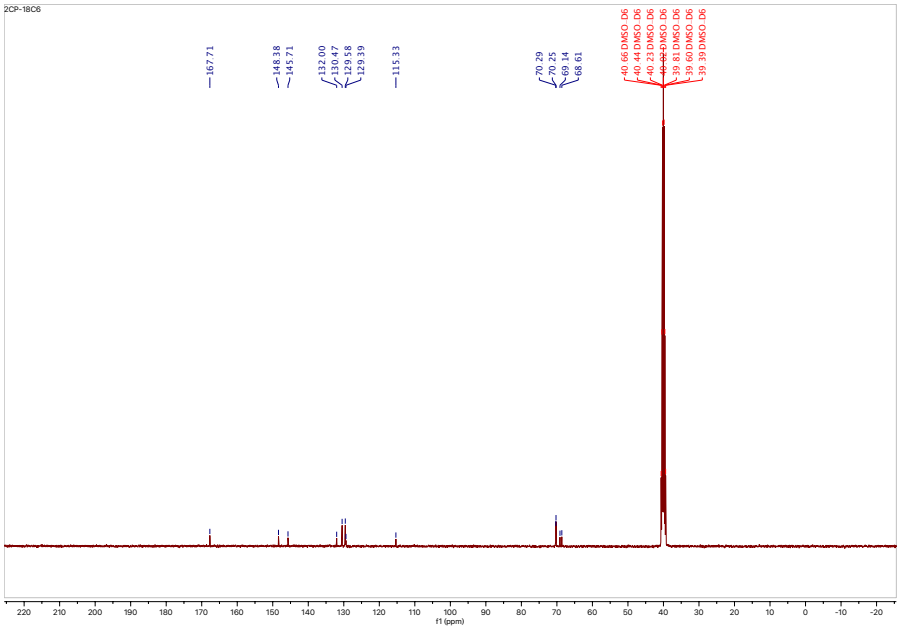

Figure 2-6. ^{13}C NMR (100 MHz, DMSO-d_6) spectrum of **1CT-18C6**.

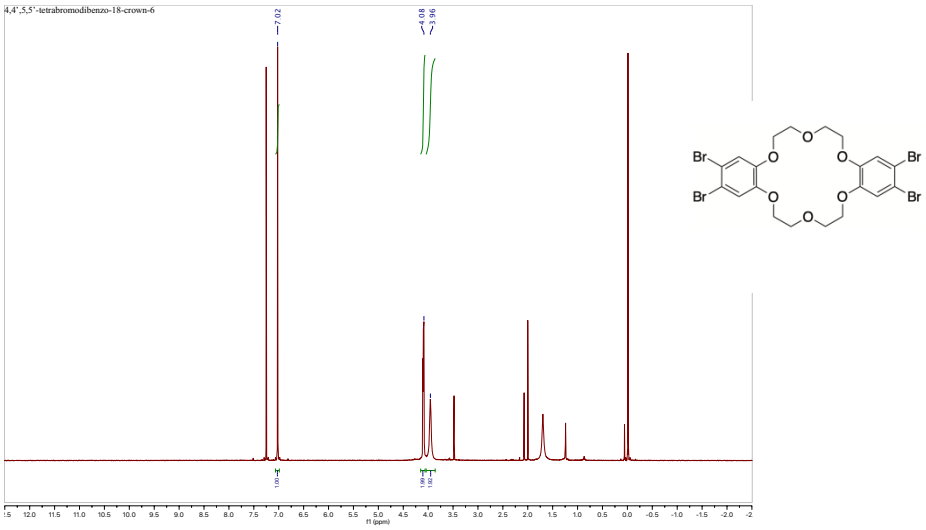

Figure 2-7. ^{1}H NMR (400 MHz, $CDCl_3$) spectrum of **4,4',5,5'-Tetrabromodibenzo-18-crown-6**.

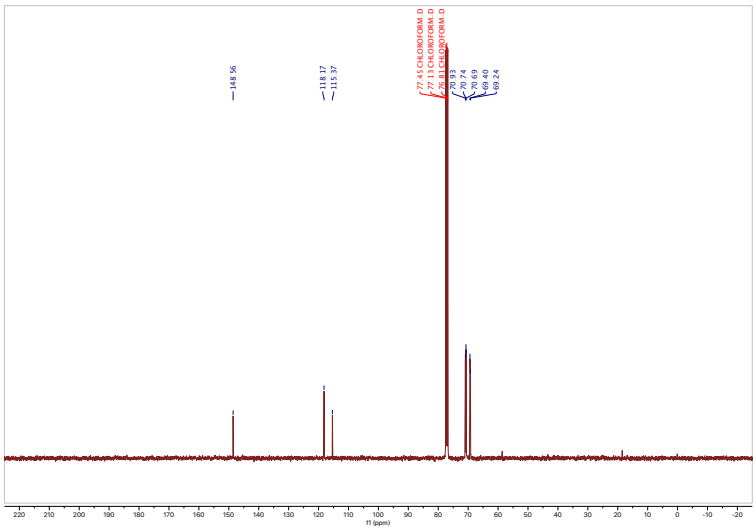

Figure 2-8. ^{13}C NMR (100 MHz, $CDCl_3$) spectrum of **4,4',5,5'-Tetrabromodibenzo-18-crown-6**.

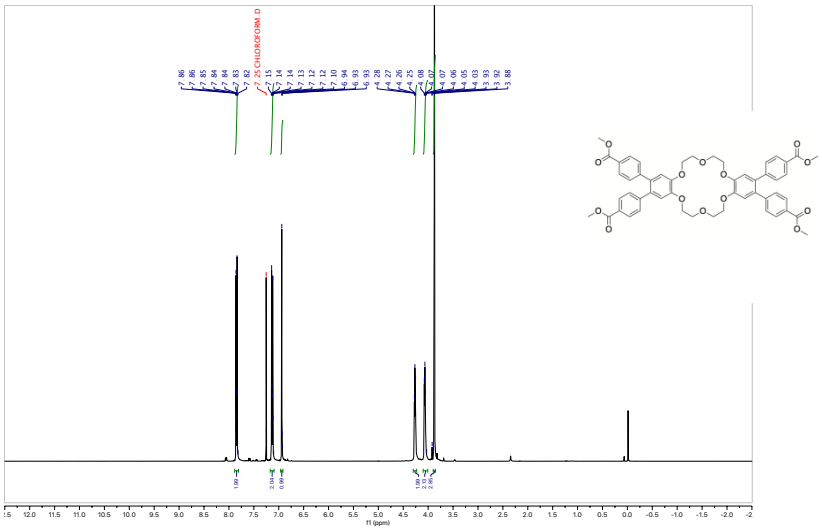

Figure 2-9. ^{1}H NMR (400 MHz, $CDCl_3$) spectrum of **2**.

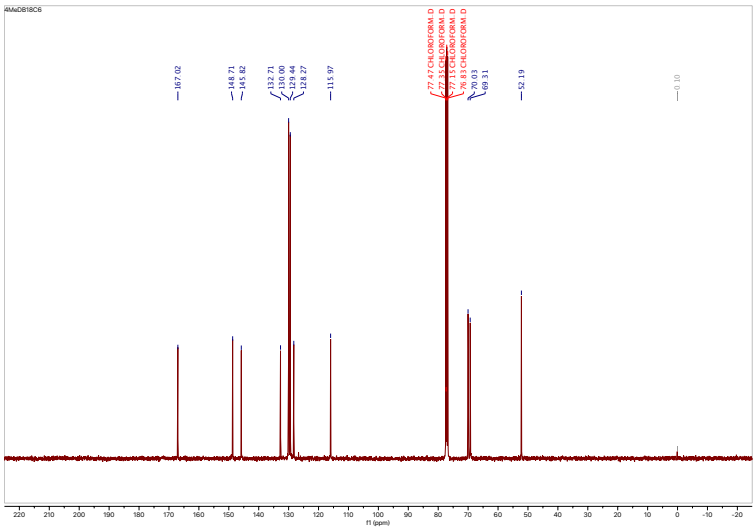

Figure 2-10. ^{13}C NMR (100 MHz, $CDCl_3$) spectrum of **2**.

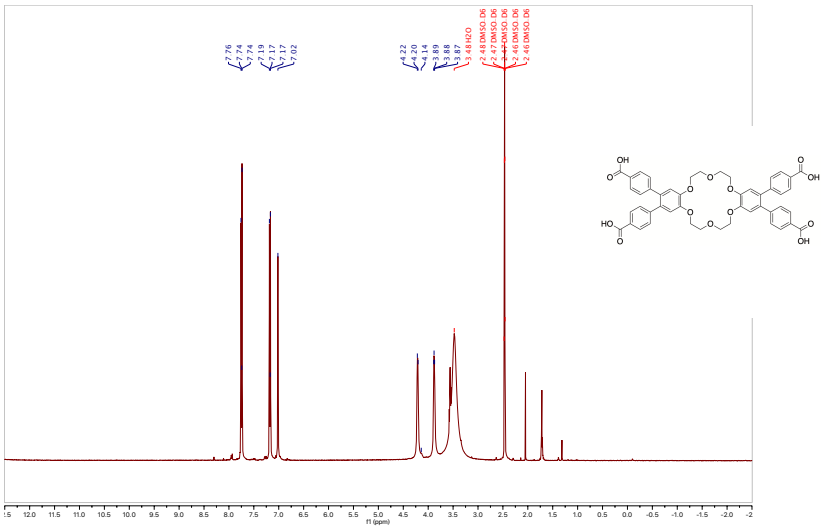

Figure 2-11. ^{1}H NMR (400 MHz, DMSO-d_6) spectrum of **2CT-18C6**.

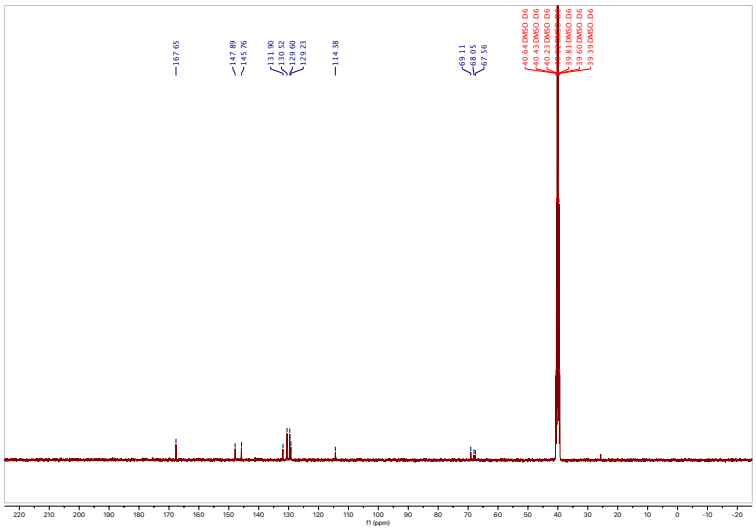

Figure 2-12. ^{13}C NMR (100 MHz, DMSO-d_6) spectrum of **2CT-18C6**.

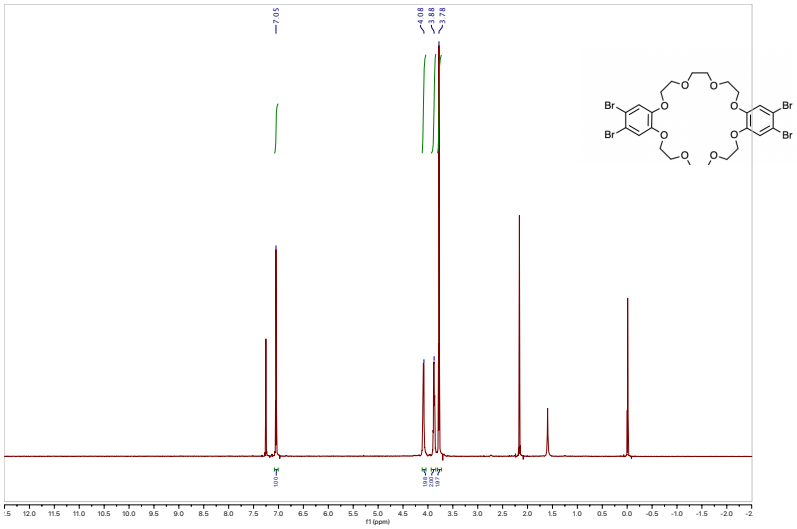

Figure 2-13. ^{1}H NMR (400 MHz, $CDCl_3$) spectrum of **4,4',5,5'-Tetrabromodibenzo-24-crown-8**.

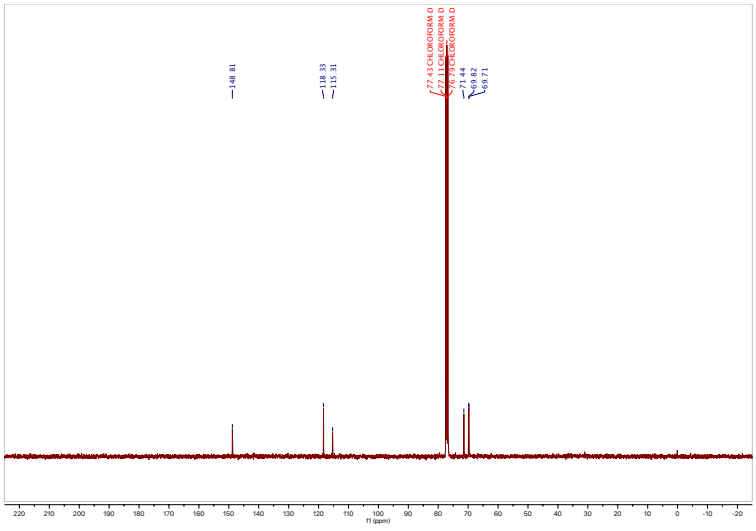

Figure 2-14. ^{13}C NMR (100 MHz, $CDCl_3$) spectrum of **4,4',5,5'-Tetrabromodibenzo-24-crown-8**.

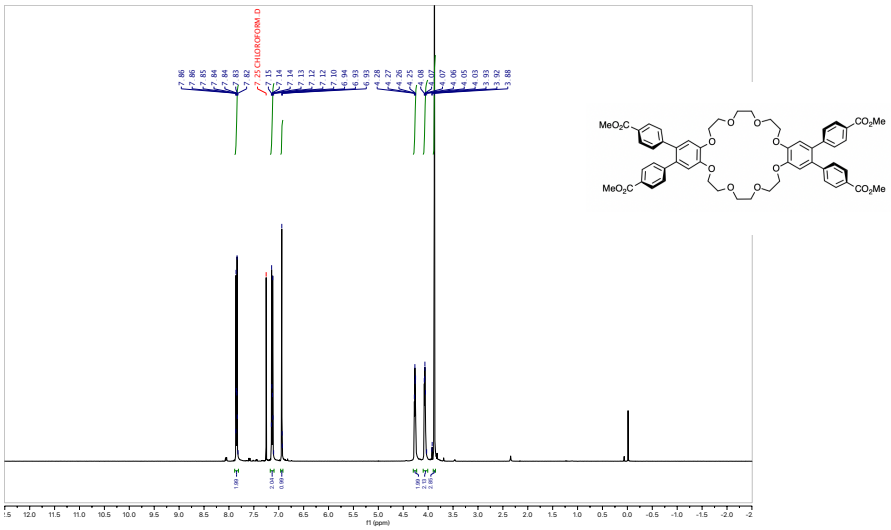

Figure 2-15. ^{1}H NMR (400 MHz, $CDCl_3$) spectrum of **3**.

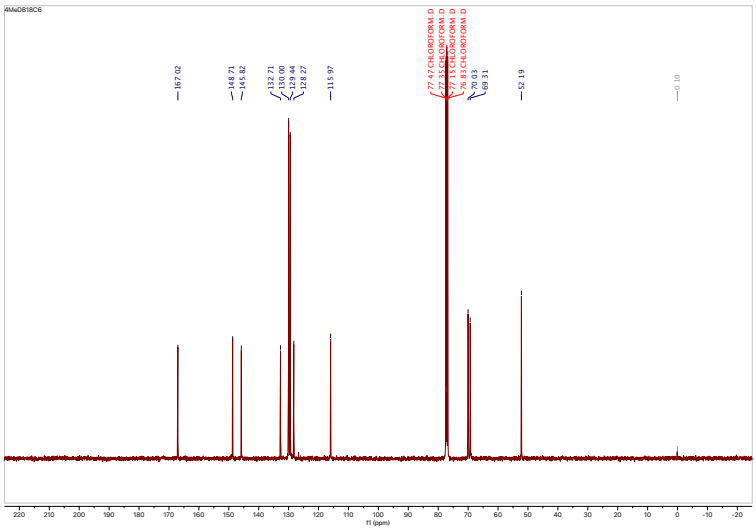

Figure 2-16. ^{13}C NMR (100 MHz, $CDCl_3$) spectrum of **3**.

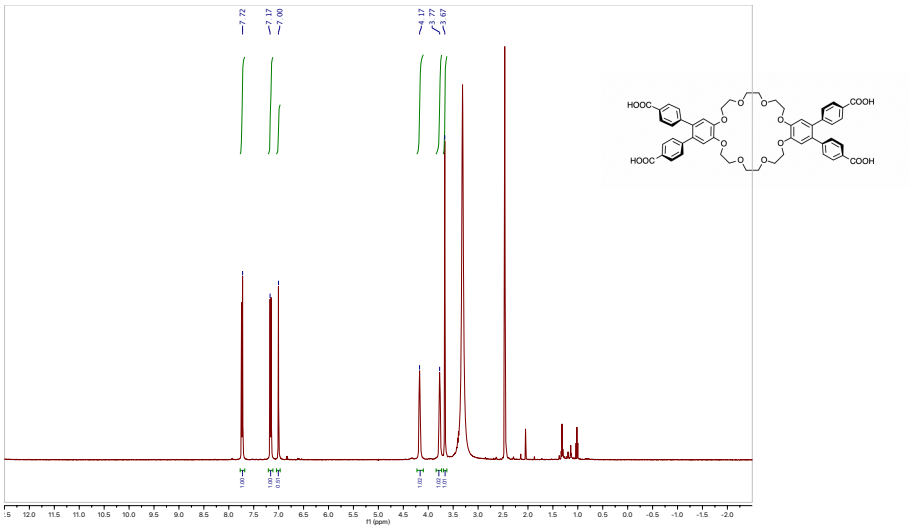

Figure 2-17. ^{1}H NMR (400 MHz, DMSO-d_6) spectrum of **2CT-24C8**.

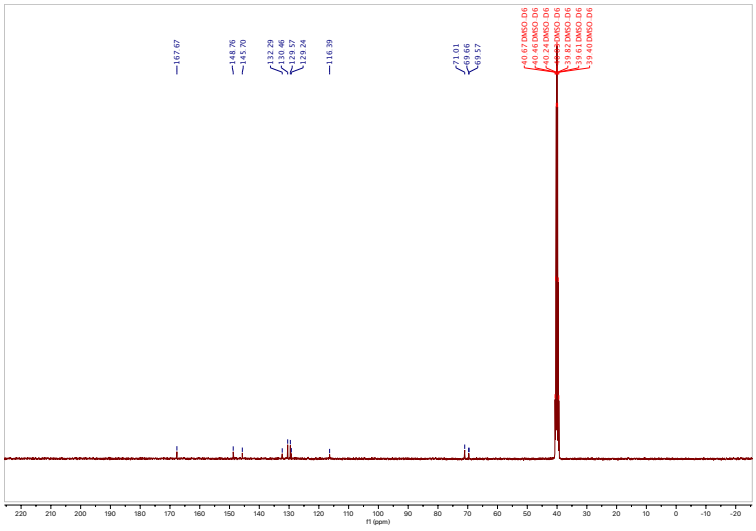

Figure 2-18. ^{13}C NMR (100 MHz, DMSO-d_6) spectrum of **2CT-24C8**.

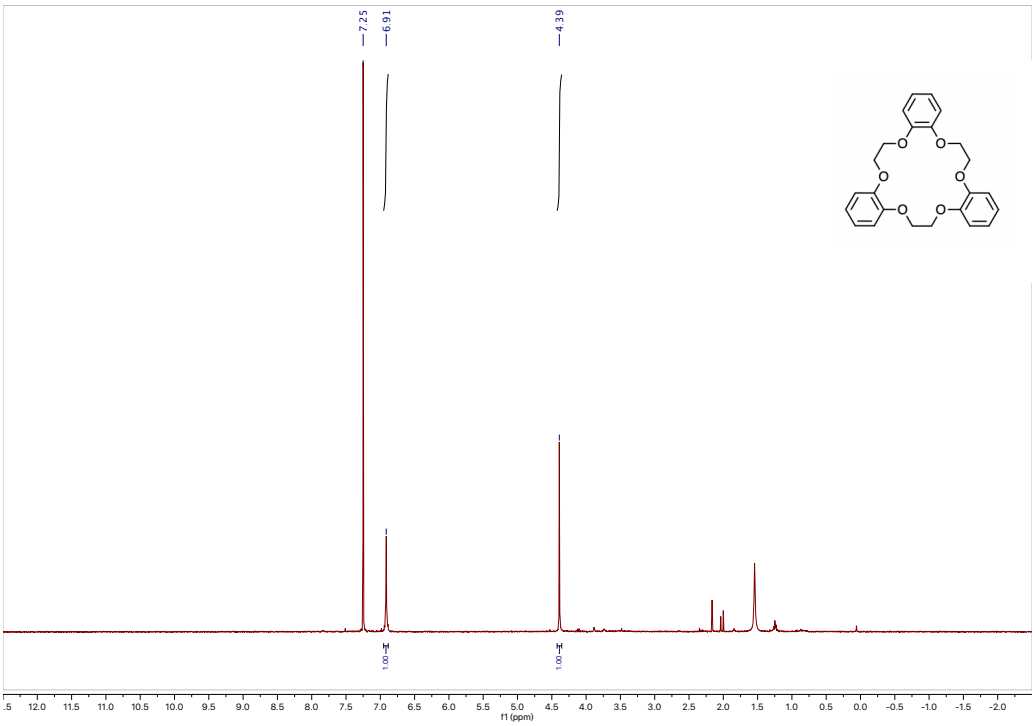

Figure 2-19. ^{1}H NMR (400 MHz, $CDCl_3$) spectrum of **4**.

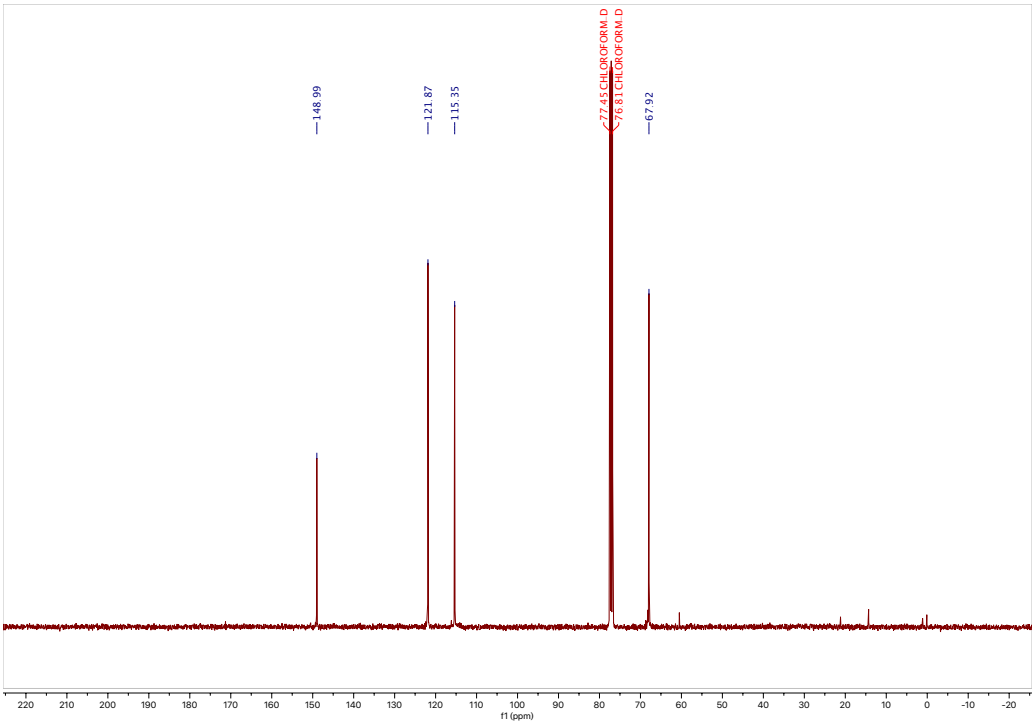

Figure 2-20. ^{13}C NMR (100 MHz, $CDCl_3$) spectrum of **4**.

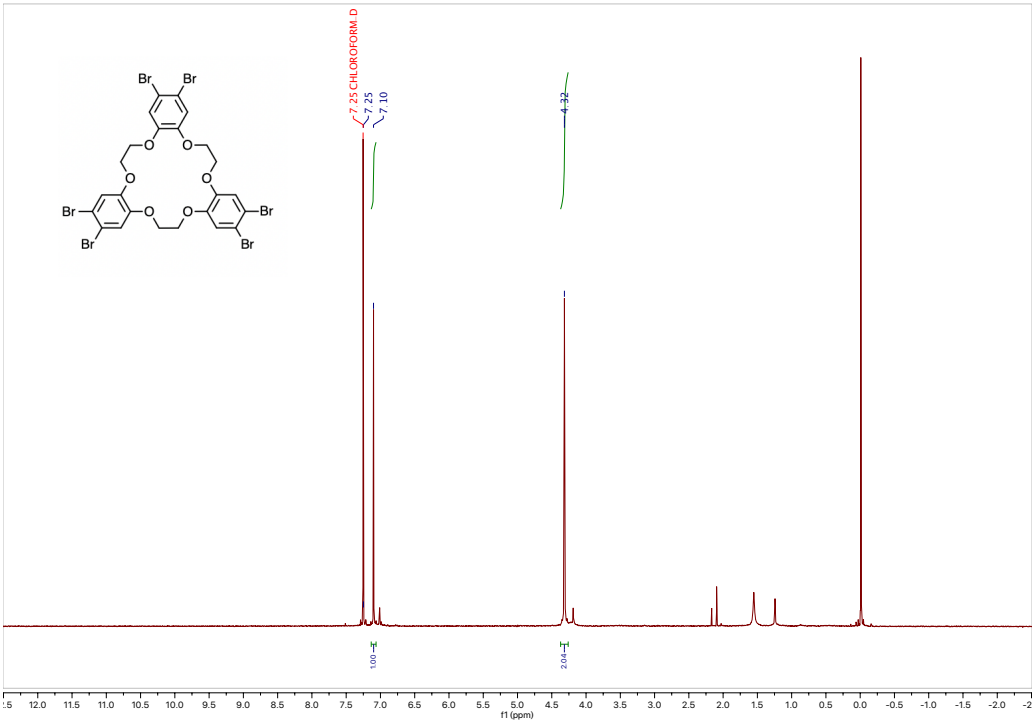

Figure 2-21. ^{1}H NMR (400 MHz, $CDCl_3$) spectrum of **5**.

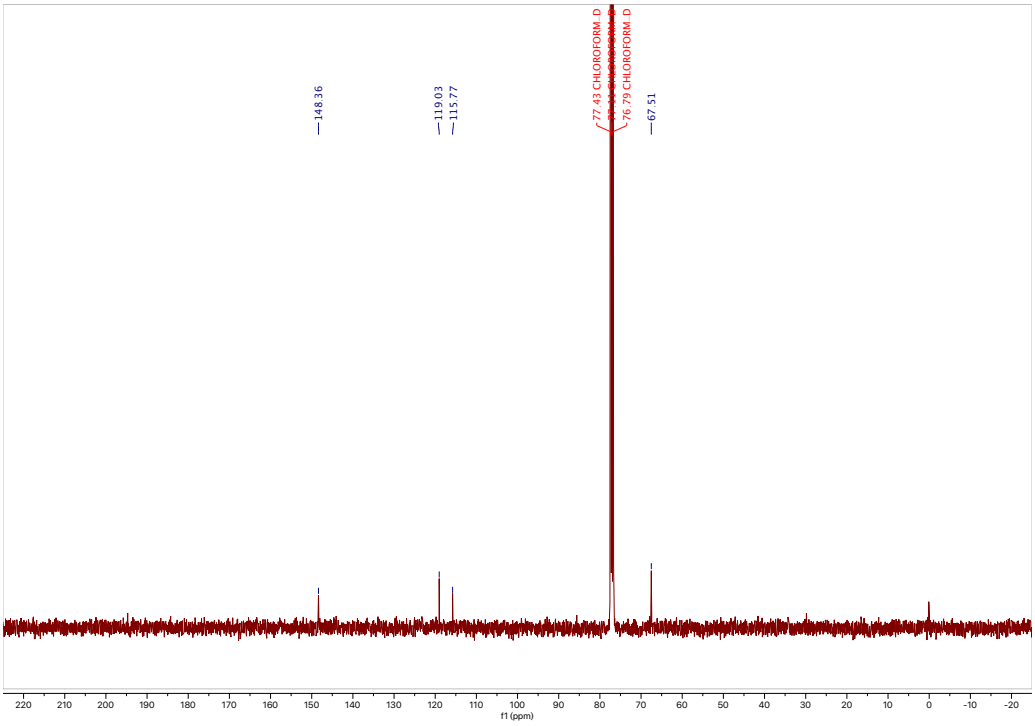

Figure 2-22. ^{13}C NMR (100 MHz, $CDCl_3$) spectrum of **5**.

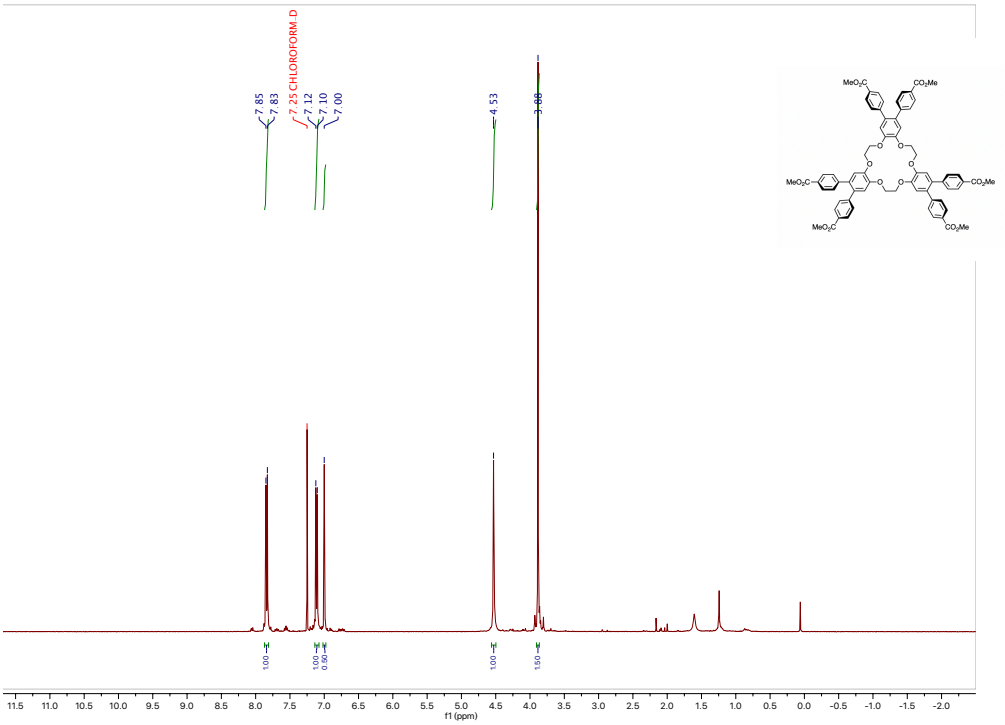

Figure 2-23. ^{1}H NMR (400 MHz, $CDCl_3$) spectrum of **6**.

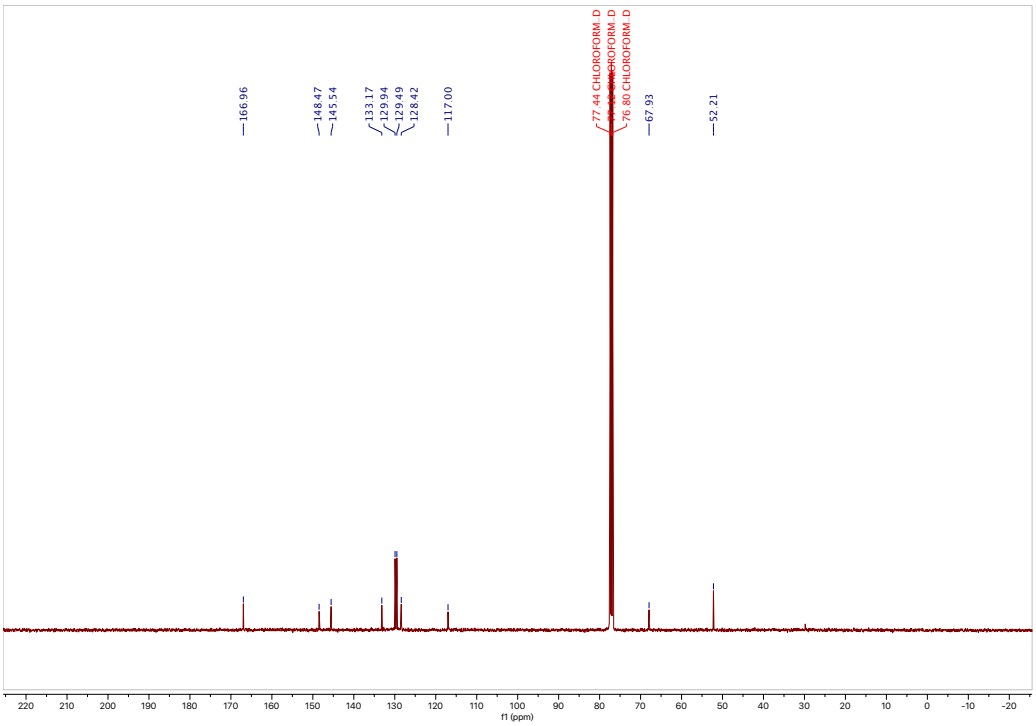

Figure 2-24. ^{13}C NMR (100 MHz, $CDCl_3$) spectrum of **6**.

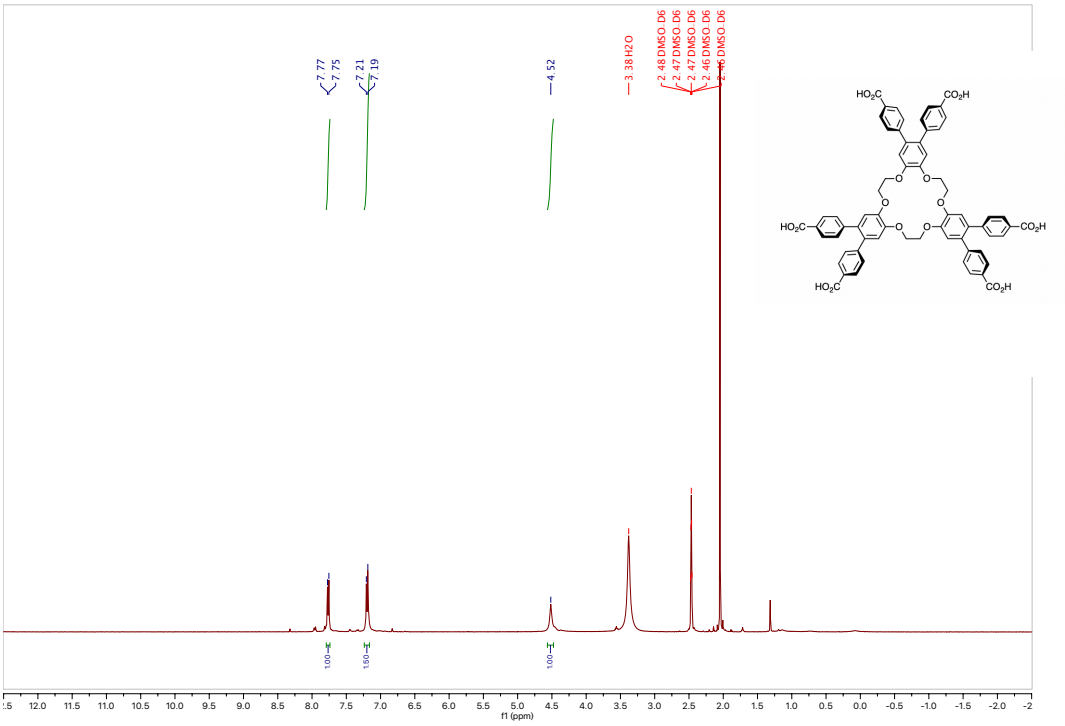

Figure 2-25. ^{1}H NMR (400 MHz, CD_3OD) spectrum of **3CT-18C6**.

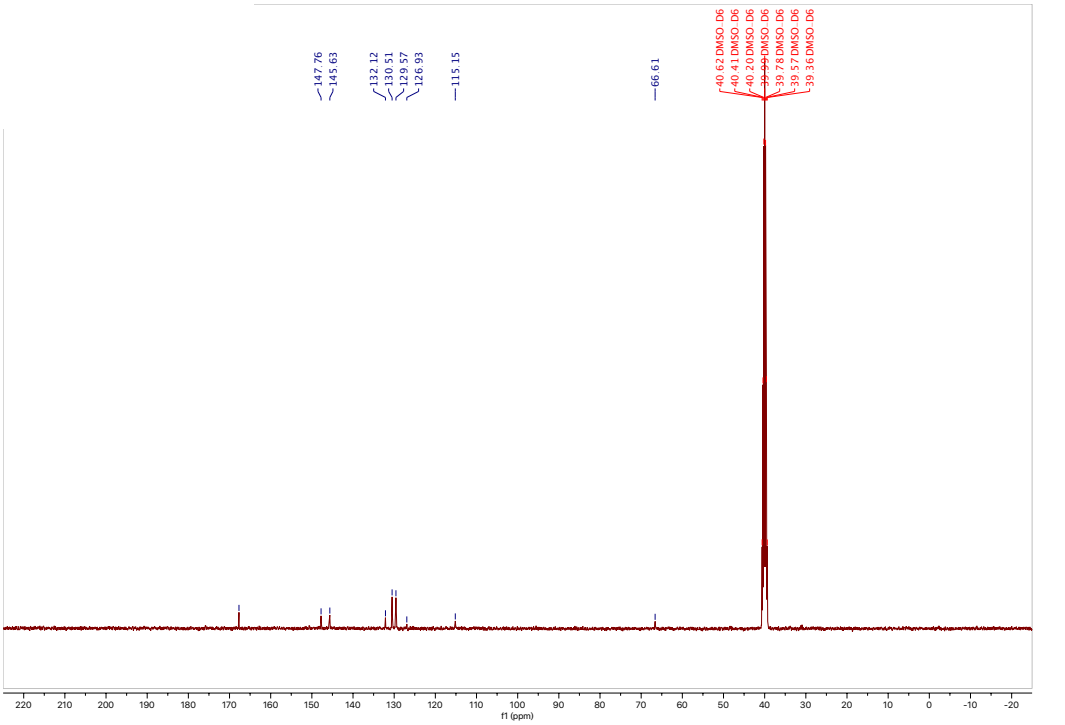

Figure 2-26. ^{13}C NMR (100 MHz, $CDCl_3$) spectrum of **3CT-18C6**.

2-7. Measurement.

Spectroscopy. Nuclear magnetic resonance (NMR) spectra were recorded in $CDCl_3$ on AV 400 MHz JEOL ECX-400 NMR spectrometers. Chemical shifts are reported in δ ppm relative to solvent peak (^{1}H NMR: δ 7.26 ppm and 2.50 ppm for $CDCl_3$ and DMSO-*d*$_6$, respectively; ^{13}C NMR: δ 77.16 ppm and 39.52 ppm for $CDCl_3$ and DMSO-*d*$_6$, respectively) with peak multiplicities described as singlet (s), broad singlet (br. s), doublet (d), triplet (t), quartet (q) and multiplet (m) in ^{1}H NMR spectra.

2-8. References

1. GeÂraud Dubois, Catherine ReyeÂ, Robert J. P. Corriu, Claude Chuit, *J. Mater. Chem.*, **2000**, 10, 1091-1098.
2. Robert E. Hanes, Jr., Edward C. Ellingsworth, Scott T. Griffin, Robin D. Rogers, Richard A. Bartsch, *ARKIVOC*, **2010**, 7, 217-237.

Chapter 3

A Proton Conductive Framework Incorporating 18Crown-6-ether and Dicarboxy-*o*-terphenyl Moieties

3-1. Abstract

In this part, the author revealed that the flexible organic 18-crown-6 derivatives with one or two 4,4'-dicarboxy-o-terphenyl (CT) groups, formed four kinds of crystals: **1CT-18C6-I** ($P2_1/n$), **2CT-18C6-I** (P-1), **2CT-18C6-II** (P-1) and **2CT-18C6-III** ($Cmc2_1$). Single crystal X-ray diffraction analysis clearly suggested the water molecules involved hydrogen-bonded network for all frameworks. In particular, a unique one-dimension (1D) pathway had formed in **2CT-18C6-III** and the activation energy (Ea) was evaluated by Arrhenius plots to be 0.14 eV, indicating that the proton jumps from H_3O^+ to the neighboring H_2O in the hydrogen-bonded network of **2CT-18C6-III**.

3-2. Introduction

Under the concept of green sustainable development, new clean fuel sources are absolutely necessary. Proton exchange membrane fuel cells (PEMFCs) are one of the most optimal technologies to alternative the common fossil fuels.[1] Proton exchange membranes (PEMs) with the ionic pathway for the protons are critical for the PEMFCs. Presently, organic conductive polymers, such as Nafion, sulfonated and phosphonic-based polyaromatics, polybenzimidazoles have been employed as the alternative PEMs materials.[2–7] They exhibit the following features required for PEMs: (a) presence of proton-conducting functionalities,[8–10] (b) poor electronic conductivities, and (c) good chemical and thermal stabilities. However, even the Nafion, achieving the outstanding proton conductivity of 10^{-1} S cm^{-1} at room temperature with 100% relative humidity (RH), still involves unavoidable defects. Thus, exploration of optimizing electrolyte materials have attracted much attention in this field.

Proton conduction in PEMs related to two mechanism, namely, the Grotthuss and vehicular mechanism.[11–13] The vehicular mechanism indicates the diffusion of protons with the vehicles. While, the Grotthuss mechanism always occurs in a water-based degenerated system consisting of H_3O^+ and H_2O within an infinite network of hydrogen bonds. A proton jumps from H_3O^+ to a neighbouring H_2O as well molecules rotations, which contribute to a high proton conductivity.

As well known, crown ether derivatives, such as dibenzo-18-crown-6-ether (DB18C6) with an excellent ability to bind alkali metal cations and water molecules, have drawn much attention as an ion conductive material.[14–16] Theoretical calculation indicated that DB18C6 with H_3O^+ ions located in the cavities of the crown ether interact with water molecules,[17–18] revealed the formation of hydrogen-bonded networks which enable proton transfer through channels and show the potential of the PEMs. However, the organic electrolyte materials based on crown ethers are hitherto unknown.

Herein, we newly designed 18-crown-6 derivatives with one and two 4,4'-dicarboxy-o-terphenyl (CT) groups, 1CT-18C6, and 2CT-18C6, respectively, as a building block molecule to develop proton conductive organic crystalline materials (Figure 3-1). A working hypothesis is as follows: (1) The 18-crown-6 and carboxy groups can capture

water molecules via hydrogen bonds; (2) The carboxy group also can form supramolecular synthon to organize the molecules into crystalline supramolecular frameworks; and (3) The rigid *o*-tephenyl moiety can provide a space for H^+ conducting and a skeleton of the framework. To date, 2CT-18C6 has been applied as an organic ligand of a metal-organic framework, proton conductive molecular crystalline materials based on 2CT-18C6 are hitherto-unknown.

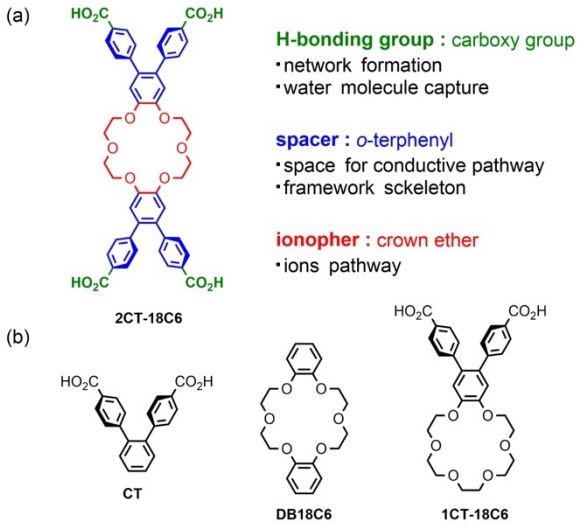

Figure 3-1. (a) A molecular structure of 2CT-18C6 and expected roles of the parts. (b) Related molecules 1CT-18C6, dibenzo-18-crown-6 (DB18C6), and CT.

2CT-18C6 are revealed to form three kinds of crystalline frameworks (**2CT-18C6-I**, **-II**, and **-III**). In particular, **2CT-18C6-III** has a unique 1D water pathway and showed the proton conductivity of 3.43×10^{-8} S cm^{-1} at 85% RH. Notably, the activation energy (*E*a) was evaluated by Arrhenius plots to be 0.14 eV, suggesting that the proton jumps from H_3O^+ to the neighboring H_2O in the H-bonding networks of **2CT-18C6-III**. The thermogravimetric analysis (TGA) also indicated that **2CT-18C6-III** is stable up to 588 K. The present system is the first example for the tailor structural features of crown ethers with a 1D water pathway.

In this part, the author presents synthesis of the crown ether derivatives, construction of crystalline frameworks, and evaluation of their H^+ conductivity. Moreover, the relationships between the structures of water pathways and proton conductivity are discussed.

3-3. Results and discussion.

Synthesis and crystallization. 4,5-Bis(methoxycarbonylphenyl)benzo-18-crown-6 (**1**) and 4,4',5,5'-tetrakis(methoxycarbonylphenyl)dibenzo-18-crown-6 (**2**) were synthesized through a Suzuki-Miyaura cross-coupling reaction of (4-(methoxycarbonyl)phenyl)boronic acid and the corresponding brominated crown ether derivatves. Hydrolysis of **1** and **2** gave 1CT-18C6 and 2CT-18C6, respectively. The details for synthesis of 1CT-18C6 and 2CT-18C6 is shown in **Chapter 2**. Condition to prepare frameworks are shown in Scheme 3-1.

Scheme 3-1. Crystallization of 1CT-18C6 and 2CT-18C6.

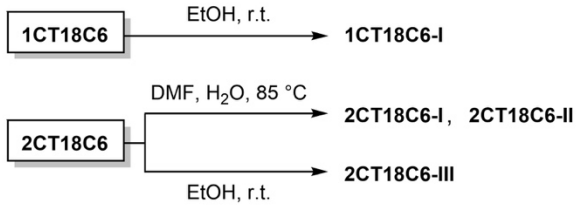

1CT-18C6 dissolved in EtOH at room temperature for 1 day afforded colorless block crystals (**1CT-18C6-I**). 2CT-18C6 forms three forms **2CT-18C6-I**, **-II**, and **-III**. Slow evaporation of a mixed solution of *N*,*N*-dimethylformamide (DMF) and water at 85 °C for several days successfully obtained two kinds of block-shaped *P*-1 crystals (**2CT-18C6-I** and **2CT-18C6-II**) concomitantly. 2CT-18C6 dissolved in EtOH at room temperature afforded a colorless block $Cmc2_1$ crystal (**2CT-18C6-III**). Crystal data of these crystals are listed in Table 3-1.

Table 3-1. Crystallographic parameters of **1CT-18C6** and **2CT-18C6.**

	1CT-18C6-I	**2CT-18C6-I**	**2CT-18C6-II**	**2CT-18C6-III**
Empirical formula	$C_{30}H_{36}O_{13}$	$C_{58.5}H_{64.5}N_{3.5}Na\ O_{17.5}$	$C_{57}H_{60}N_3NaO_{17}$	$C_{48}H_{42}O_{17}$
Guest species	H_2O	Na^+, DMF	Na^+, DMF	H_2O
Formula weight	604.59	1119.62	1082.07	890.81
Temperature/K	223	293	293	298
Crystal system	monoclinic	triclinic	triclinic	orthorhombic
Space group	$P2_1/n$	*P*-1	*P*-1	$Cmc2_1$
a / Å	13.6633(2)	11.3113(2)	13.1094 (8)	27.4687(10)
b / Å	8.2601(1)	13.4267(2)	25.3405(16)	20.3236(8)
c / Å	26.8789(6)	21.7047(4)	26.7457(16)	8.0251(6)
α / °	90	104.103(2)	105.281(5)	90

β / °	90.208(2)	95.2670(10)	90.128(5)	90
γ / °	90	111.048(2)	91.834(5)	90
V / Å^3	3033.54(9)	2924.57(10)	8565.8(9)	4480.1(4)
Z	4	2	6	4
F (000)	1280	1138	3408	1864
F^2	1.029	1.059	0.901	1.034
R_1 [a], wR_2 [b][I > 2σ(I)]	0.059, 0.184	0.061,0.209	0.081, 0.352	0.094, 0.288
CCDC *No*.	2057700	2078832	2078834	2078835
* [a] $R_1 = \sum\|\|F_o\| - \|F_c\|/\sum\|Fo\|$. [b] w$R_2 = \{\sum[w(F_o^2 - F_c^2)^2]/\sum[w(F_o^2)^2]\}^{1/2}$				

Crystallography.

In **2CT-18C6-I** crystal, a sodium cation is captured at the center of the crown ether with a Na^+•••O distance ranging from 2.57 to 2.79 Å. Two DMF molecules are then coordinated to the Na^+ from axial directions. Because of the cation binding, the 18C6 moiety has a boat-shape conformation with bent angle of 71.2° (Figure 3-2a), where the bending angle defined as a dihedral angle between the mean planes of the two benzene rings of the dibenzo-18-crown-6-ether moiety. Three of the four carboxy groups form intermolecular hydrogen bonds and the one binds to a DMF molecule, resulting formation of a ribbon like motif (Figure 3-2b). It is noteworthy that the carboxy groups form no self-complementary dimer, which is often observe in hydrogen bonded frameworks composed of highly-symmetric rigid pi-conjugated molecules[19], but branched networks as shown in Figure 3-2c. This result clearly indicates that flexibility and lower symmetry of **2CT-18C6-I** crucially effects on a way of formation of a hydrogen bonded network. Packing of the boat shape molecules provides small inclusion spaces, in which water and DMF molecules are included. In this framework, however, there are no one-dimensional water alignment suitable for proton conduction.

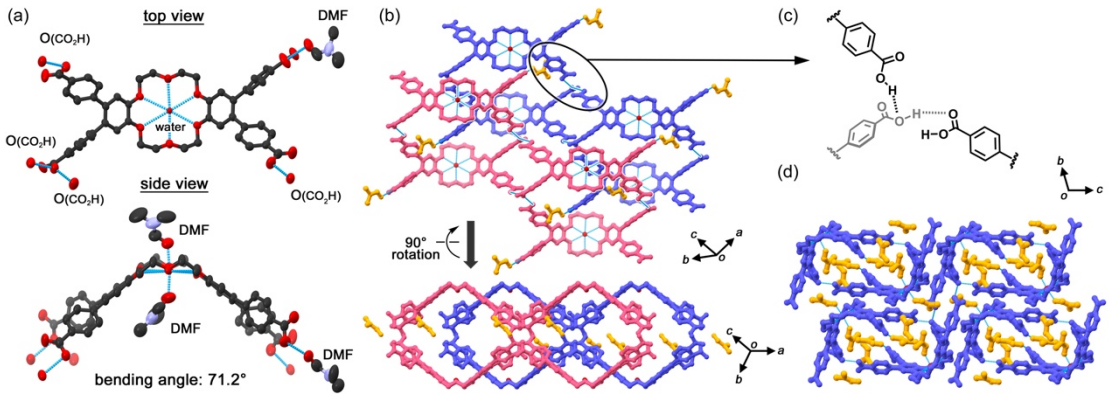

Figure 3-2. Crystal structure of **2CT-18C6-I.** (a) Anisotropic Ellipsoid plot with 50% probability. (b) One-dimensional ribbon-like motifs formed through intermolecular hydrogen bonds. (c) Blanched Hydrogen bonded network formed by three carboxy groups and water molecules. (d) Packing diagram, where water and DMF molecules are colored by red and orange, respectively.

2CT-18C6-II consists of crystallographically independent three molecules as well as DMF molecules. **2CT-18C6-II** has almost the same structure with **2CT-18C6-I**. (Figure 3-3)

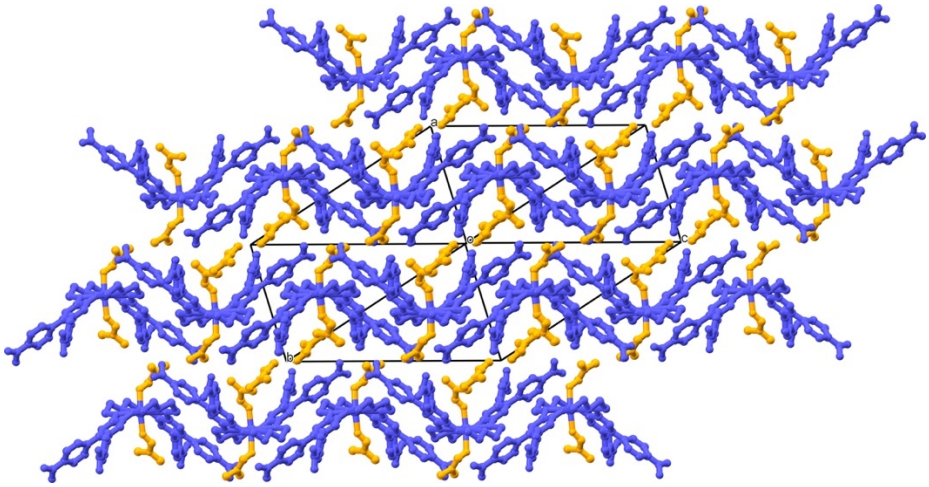

Figure 3-3. Crystal structure of **2CT18C6-II**.

In **2CT-18C6-III** crystal, a C_s-symmetric 2CT-18C6 molecule has quite shallow boat conformation with a bent angle of 25.2° (Figure 3-4a). The carboxy groups form hydrogen bonds with only water molecules to give the crystal contains no solvent but water molecules with a host/guest ratio of 1 : 5 stoichiometry (Figure 3-4b). One water molecule form hydrogen bond with crown ether's oxygen and the carboxy groups with 2.86 Å and 2.69 Å, respectively, and is isolated from neighboring water molecules (yellow spheres). The other four molecules (red spheres), on the other hand, form

hydrogen bonds with the carboxy groups (O•••O distances: 2.72, 2.89, and 2.94 Å) to form one-dimensional zig-zag alignment along the *c* axis (Figure 3-4c). Distance between the oxygen atoms of the neighboring water molecules is 2.97 Å and 3.74 Å (Figure 3-4d).

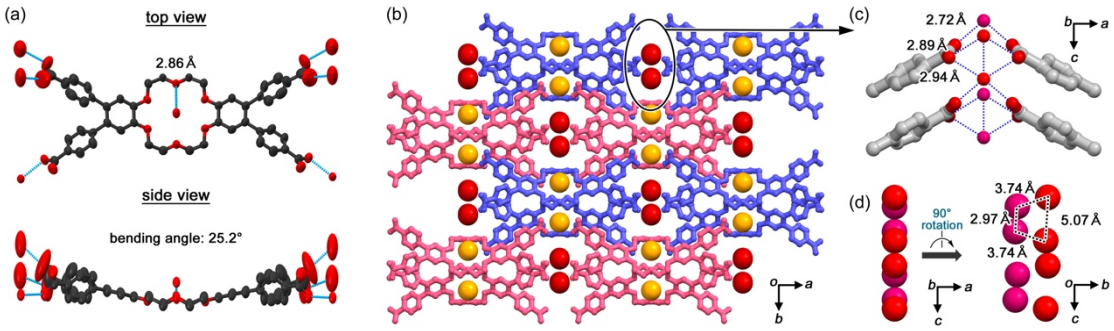

Figure 3-4. Crystal structure of **2CT-18C6-III.** (a) Anisotropic Ellipsoid plot with 50% probability. (b) Packing diagram, where two types of water molecules are colored with red and orange. (c) Hydrogen bonds among carboxy groups and water molecules. (d) Alignment of waters in channel with intermolecular distances.

1CT-18C6-I also contains only water molecules with a host/guest ratio of a 1 : 3 stoichiometry. Two water molecules are hydrogen bonded by the crown ether's oxygen atoms and the other are by the carboxy groups. Totally, the water molecules are aligned one dimensionally along the *b* axis. The distance between oxygen atoms of the neighboring water molecules ranges 2.77 to 3.68 Å. Although these distances are relatively shorter than that in the case of **2CT-18C6-III**, the alignment crosses through crown ether ring (Figure 3-5).

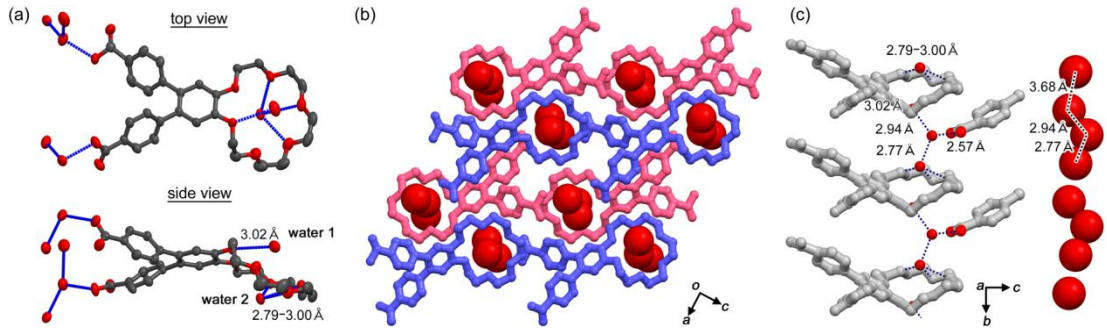

Figure 3-5. Crystal structure of **1CT-18C6-I.** (a) Anisotropic Ellipsoid plot with 50% probability. (b) Packing diagram, where water molecules are shown by the space-fill model. (c) Hydrogen bonds among the crown ether, carboxy groups, and water molecules. (d) Alignment of waters in channel with intermolecular distances.

Phase purity and thermal stability.

The powder X-ray diffraction (PXRD) patterns of crystalline bulk samples of **1CT-18C6-I** and **2CT-18C6-III** are in good agreement with the ones simulated from their single-crystal data respectively (Figure 3-6), indicating high phase purity and good stability. The thermogravimetric analysis (TGA), **1CT-18C6-I** starts losing slowly from room temperature and displays 8.9% weight loss to 373 K, which corresponds to the loss of the water molecules (cal. 8.9%). Then the framework maintains until 588 K (Figure 3-6a). Similarly, **2CT-18C6-III** shows a 4.5% weight loss of water molecules from room temperature to 373 K (cal. 6.0%) and the framework also collapses after 588 K (Figure 3-6b). On the other hand, variable temperature-PXRD plots shows both **1CT-18C6-I** and **2CT-18C6-III** with an obvious change of structure with the increase of the temperature, which result from the reorganization of the hydrogen bonds connected with the loss of the water molecules (Figure 3-6c, 3-6d).

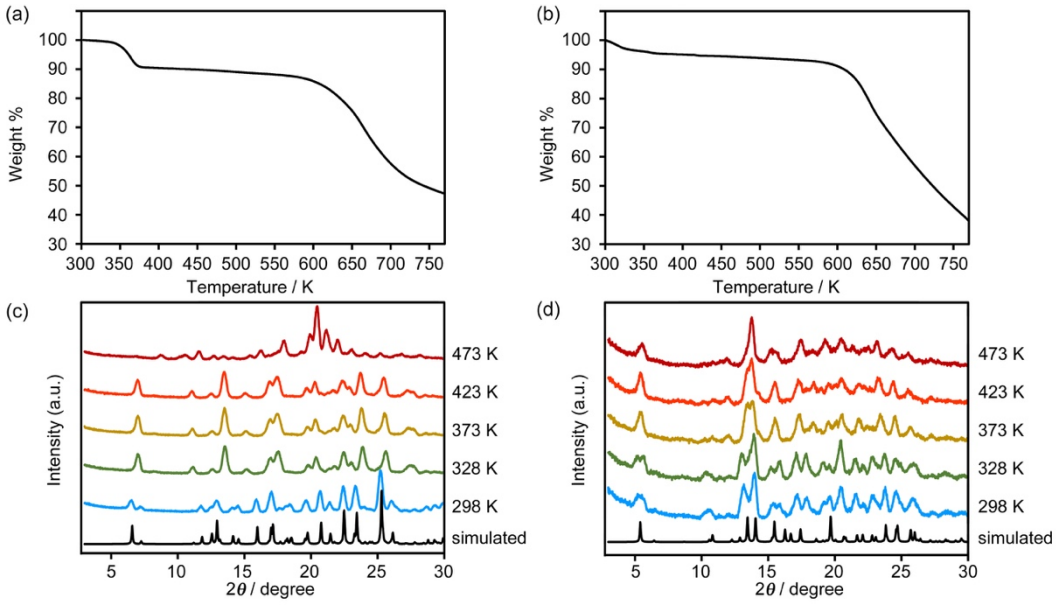

Figure 3-6. TG plots of as-formed crystals of (a) **1CT-18C6-I** and (b) **2CT-18C6-III**. Variable temperature (VT-) PXRD patterns of (c) **1CT-18C6-I** and (d) **2CT-18C6-III**, where simulated patterns based on SXRD analysis were at the bottom.

Proton Conductivity.

The structures of **1CT-18C6-I** and **2CT-18C6-III** were constructed by hydrophilic crown ether moiety, assembly of carboxy groups, and one-dimensional alignment of water molecules. In addition, TG and variable temperature-PXRD analyses suggested the frameworks of **1CT-18C6-I** and **2CT-18C6-III** maintained after the removal of water molecules. These results indicated that there were enough sites for water molecules supplied at higher relative humidity. These structural features could provide an orderly way for proton transport. Therefore, **1CT-18C6-I** and **2CT-18C6-III** are expected to show proton conductivity. Due to the limitation of the size of the samples, compressed pellet of the samples was used for the measurement for proton conductivity. As a reference, proton conductivity at the same condition was measured for pelletized samples of 1,2-(4-carboxyphenyl)-benzene (CT) and dibenzo[18]crown-6 (DB18C6).

Temperature-dependent Nyquist plots[20–22] and the fitting parameters of equivalent circuit model for four samples of **1CT-18C6-I**, **2CT-18C6-III**, CT, and DB18C6 were summarized in Figures 3-7, 8, 9, and 10, Table 3-2, 3, 4 and 5, respectively.

1CT-18C6-I

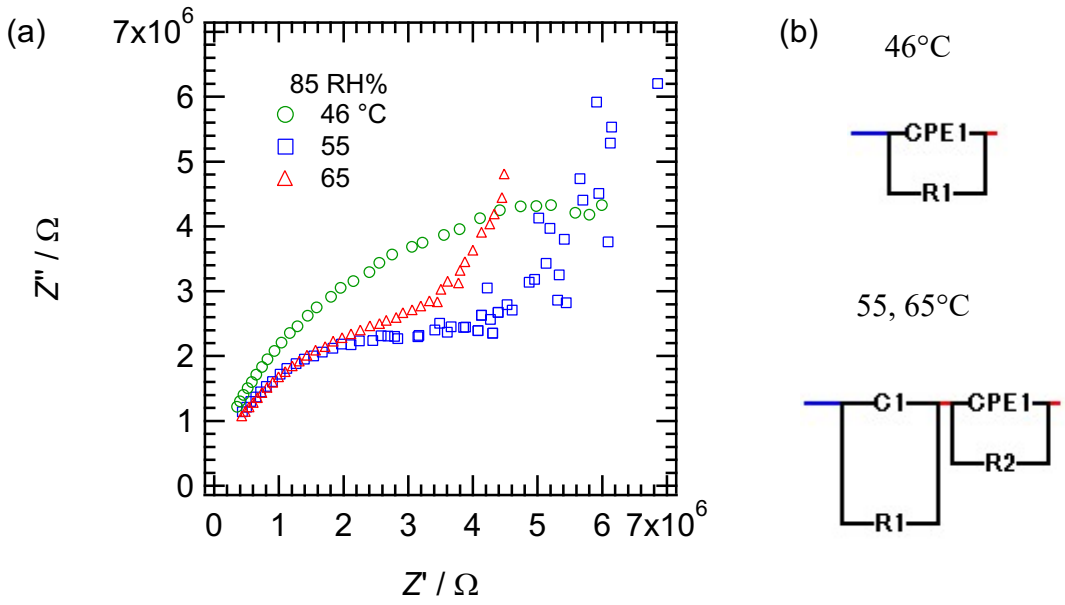

Figure 3-7. (a) Nyquist plot for **1CT-18C6-I** at 46, 55, and 65 °C under 85 RH% humidity and (b) equivalent circuit models for the fitting to data of 46 °C (top) and 55 and 65 °C (bottom).

Table 3-2. Fitting parameters of equivalent circuit model at each temperature for **1CT-18C6-I.**

T / °C	R_1 / Ω	C_1 or CPE_1 / F ^{n1}	n_1	R_2 / Ω	C_2 / F
46	1.148×10^{7}	2.025×10^{-12}	0.822	---	---
55	5.439×10^{6}	1.639×10^{-12}	0.839	3.297×10^{7}	3.538×10^{-12}
65	4.420×10^{6}	1.329×10^{-12}	0.852	3.718×10^{7}	1.329×10^{-12}

2CT-18C6-III

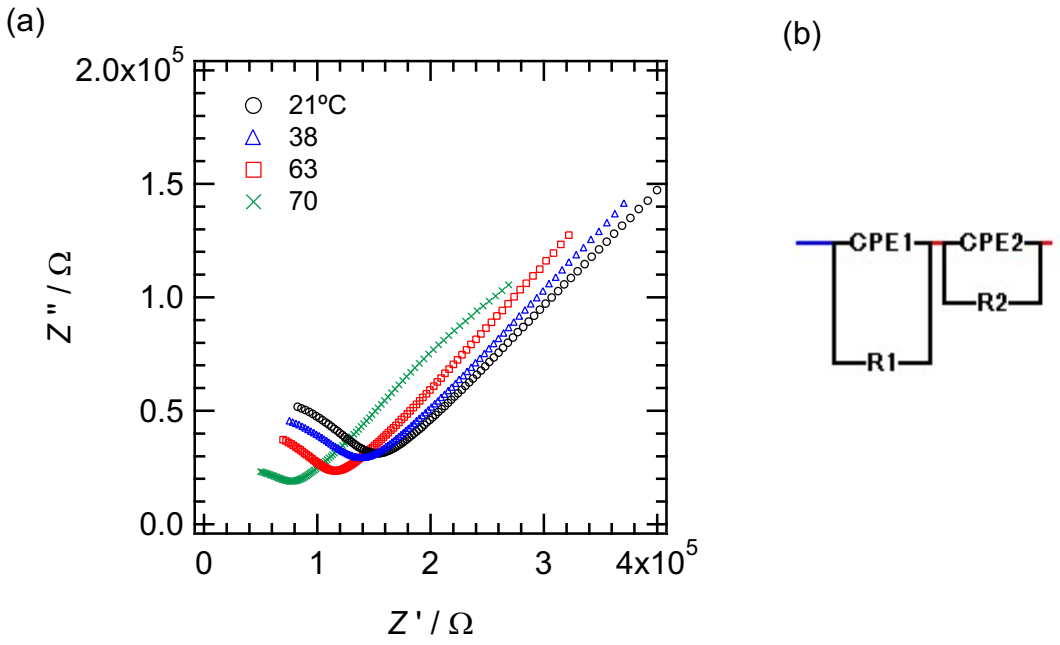

Figure 3-8. (a) Nyquist plot for **2CT-18C6-III** at 25, 63, 66, and 75 °C under 85 RH% humidity and (b) equivalent circuit models for the fitting to data.

Table 3-3. Fitting parameters of equivalent circuit model at each temperature for **2CT-18C6-III.**

T / °C	R_1 / Ω	CPE_1 / F ^{n1}	n_1	R_2 / Ω	CPE_2 / F ^{n1}	n_2
21	1.138×10^{5}	2.591×10^{-11}	0.803	2.818×10^{6}	3.788×10^{-7}	0.312
38	1.040×10^{5}	5.245×10^{-11}	0.764	1.000×10^{10}	4.666×10^{-7}	0.304
66	6.712×10^{4}	3.903×10^{-10}	0.642	6.474×10^{5}	6.876×10^{-8}	0.456
70	6.432×10^{4}	3.940×10^{-10}	0.651	1.895×10^{6}	4.170×10^{-10}	0.346

4,4'-Dicarboxy-o-tephenyl (CT)

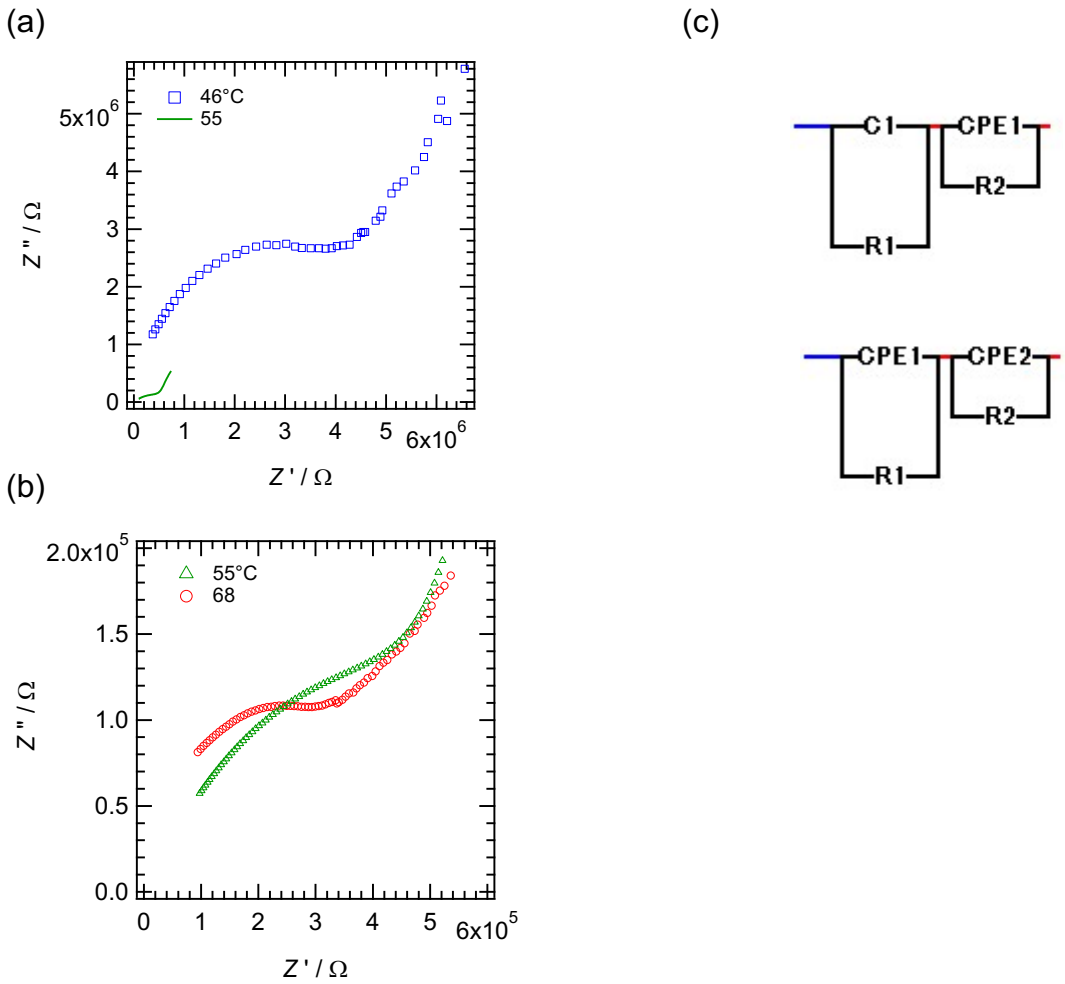

Figure 3-9. (a) Nyquist plot for CT at 46, 55, and 68 °C under 85 RH% humidity and (b) equivalent circuit models for the fitting to data of 46 °C (top) and 55 and 68 °C (bottom).

Table 3-4. Fitting parameters of equivalent circuit model at each temperature for **4,4'-Dicarboxy-o-tephenyl (CT).**

T / °C	R_1 / Ω	C_1 or CPE_1 / F	n_1	R_2 / Ω	C_2 or CPE_2 / F	n_2
46	4.594×10^{6}	1.472×10^{-13}	---	1.491×10^{7}	1.604×10^{-12}	---
55	6.584×10^{5}	8.921×10^{-9}	0.433	1.776×10^{6}	9.584×10^{-10}	---

68	2.876×10^{5}	4.026×10^{-10}	0.631	1501×10^{6}	3.793×10^{-8}	0.451

Dibenzo[18]crown-6 (DB18C6)

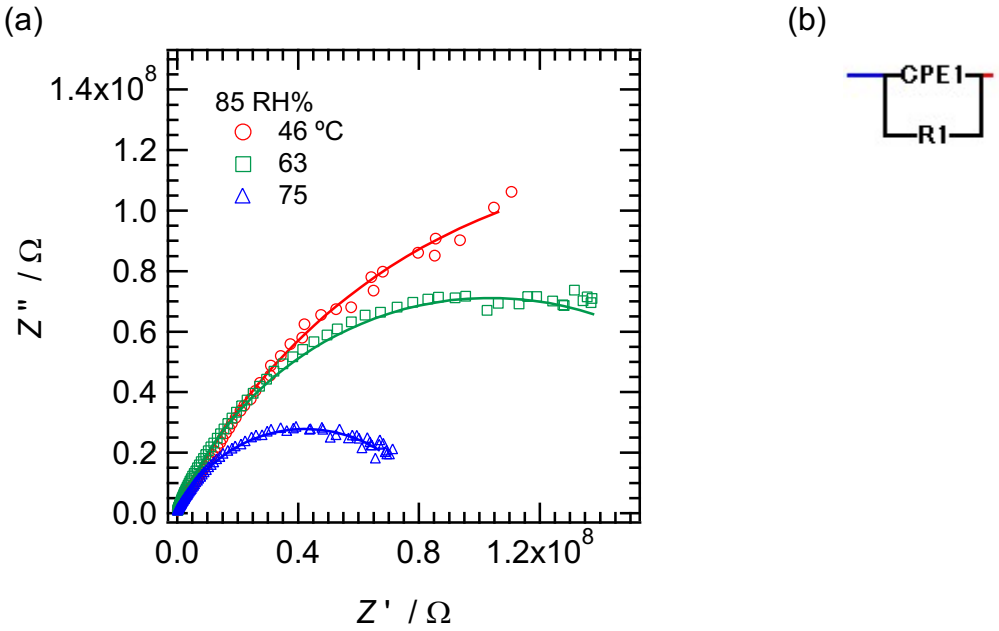

Figure 3-10. (a) Nyquist plot for DB18C6 at 46, 63, and 75 °C under 85 RH% humidity and (b) equivalent circuit models for the fitting to data.

Table 3-5. Fitting parameters of equivalent circuit model at each temperature for DB18C6.

T / °C	R_1 / Ω	CPE_1 / F ^{n1}	n_1
46	3.492×10^{8}	1.231×10^{-11}	0.727
63	2.071×10^{8}	5.191×10^{-12}	0.766
75	8.473×10^{7}	1.124×10^{-11}	0.740

The Nyquist plots (Figures 3-7, 8 and 9) of **1CT-18C6-I**, **2CT-18C6-III**, and CT were the sum of a straight line and a semicircle in the low and high frequency range, respectively. On the other hand, each Nyquist diagram of DB18C6 was composed of a single semicircle (Figure 3-10). Since the pellet sample was used to measure the proton

conductivity, the Nyquist plot showed the proton conductions which are contributed from a bulk and an interface. Since bulk conduction is usually observed in the higher frequency range than the interface[20–21] the semicircles in the Nyquist diagram of **1CT-18C6-I**, **2CT-18C6-III**, and CT were attributed to bulk conduction. For the calculation of proton conductivity, we applied the equivalent circuit model. The model for the conductivity of DB[18]crown-6 is that a resistor and constant phase element (CPE) are arranged in parallel, while the model for that of **1CT-18C6-I**, **2CT-18C6-III**, and CT is that two parallel pairs of resistors and CPEs were lined up in series.

Regarding the conductivity estimated from the equivalent circuit model, an Arrhenius plot was created from the bulk conductivity of **1CT-18C6-I**, **2CT-18C6-III**, CT, and the conductivity of DB18C6 (Figure 3-11). From the Arrhenius plot, the proton conductivities and activation energies (E_a) of **1CT-18C6-I**, **2CT-18C6-III**, CT, and DB18C6 were estimated, and summarized in Table 6. The proton conductivity at room temperature was higher in the order of **2CT-18C6-III**, **1CT-18C6-I**, CT, and DB18C6, while the E_a was lower in the order of **2CT-18C6-III**, **1CT-18C6-I**, DB18C6, and CT. The proton conductivities of MFM-511 and MFM-512, which are the MOF samples with the carboxyl group involved in proton transport, are 4.0×10^{-8} (87 RH%) and 2.5×10^{-7} S cm^{-1} (77 RH%) at 298 K, respectively. The value of proton conductivity from **2CT-18C6-III** is in the similar order of MFM-511 and MFM-512.

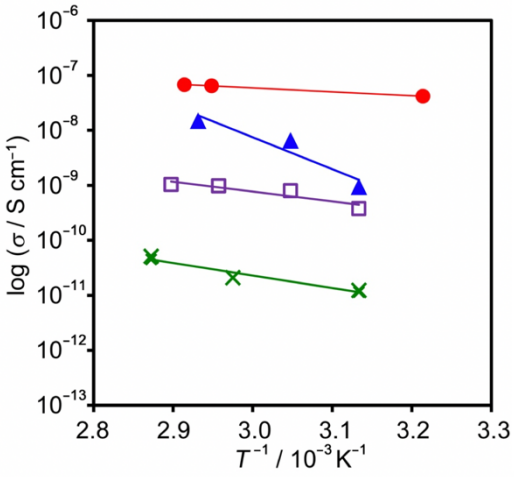

Figure 3-11. Arrhenius plot for proton conductivities under 85 RH% of **1CT-18C6-I** (purple), **2CT-18C6-III** (red), CT (blue), and DB18C6 (green).

Referring to the proton diffusion motion, proton conduction can be classified as the vehicle and the Grotthuss mechanisms, which are divided by E_a = 0.4 eV. When E_a is larger and smaller than 0.4 eV, proton conductivity is estimated to be the vehicle and Grotthus mechanisms, respectively

Since E_a of DB18C6 and CT are higher than 0.4 eV, proton conducting mechanism of DB18C6 and CT is attributed to the vehicle one. On the other hand, **1CT-18C6-I** and **2CT-18C6-III** had lower E_a than 0.4 eV, and the proton conduction of them is due to the Grotthuss mechanism (Table 3-6). Both **1CT-18C6-I** and **2CT-18C6-III** had continuous hydrogen-bonded networks, resulting in the most effective proton-conducting pathways and corresponding to Grotthus mechanism. Notably, **2CT-18C6-III** has two unique linear water pathways. Water molecules in **2CT-18C6-III** were not only arranged along the one-dimensional array of the crown ether unit, but also arranged in the parts formed the hydrogen-bonded networks surrounded by carboxy group. Therefore, **2CT-18C6-III** exhibited the highest proton conductivity of 3.43×10^{-8} S cm^{-1} under 85 RH% at 300 K.

Table 3-6. Proton conductivity at 300 K and activation energy of **1CT-18C6-I, 2CT-18C6-III,** CT, and DB18C6, estimated from Arrhenius Plot.

	σ @300 K / S cm^{-1}	E_a / eV
1CT-18C6-I	1.95×10^{-10}	0.354
2CT-18C6-III	3.43×10^{-8}	0.140
CT	8.69×10^{-11}	1.150
DB18C6	3.97×10^{-12}	0.452

3-4. Conclusions

In this study, we newly applied 18-crown-6 derivatives with one or two 4,4'-dicarboxy-o-terphenyl moieties as building block molecules to develop organic crystalline materials with proton conductivity. The 18-crown-6 and carboxy groups

capture water molecules via hydrogen bonds and constructed good self-adaptability to water molecules frameworks especially for **2CT-18C6-III** with a unique 2D water pathway, which provide available space for H^+ conduction. Based on this study, it is available to develop a novel proton conductive flexible framework with good adaptability to guest molecules. In addition, the high chemical stability and superior thermal stability indicate a promising and potential application in PEMFCs.

3-5. Measurement

Thermogravimetric analysis (TGA) was conducted using a Rigaku Thermo Plus TG8120 with a heating rate of 5 K/min under nitrogen. PXRD were measured with a Rigaku RINT2100 in the 2θ region of 5–50°. The measurements were performed with Cu K_α radiation (λ = 1.5418 Å) at scanning rate of $1.2° \cdot min^{-1}$ under an applied electric voltage and current of 40 KV and 40 mA, respectively.

Single crystalline X-ray diffraction data was collected by Rigaku MicroMax-007HF diffractometer with a Pilatus 200K detector and Cu K_α radiation (λ = 1.54184 Å) at 223 K. Analytical and multi-scan absorption corrections were applied to the reflection data. A single crystal was mounted on MicroMounts™ tip (MiTeGen) with Paratone® 8277 (Hampton Research). Data collection, cell refinement, and data reduction were carried out with Crysalis ^{PRO} (Rigaku Oxford Diffraction, 2017). The initial structure was solved by using SHELXT, and structural refinement was performed by using full-matrix least-squares techniques on F^2 using Crystal structure software (Rigaku). Anisotropic refinement was applied to all atoms except for hydrogens. SQUEEZE function equipped in the PLATON program was used to remove severely disordered solvent molecules in voids. These data are provided free of charge in The Cambridge Crystallographic Data Centre (CCDC-2057700, 2078832, 2078834, 2078835).

Frequency-dependent impedance spectra were measured using an impedance analyzer 4294A (Agilent) with four-probe AC impedance method at a frequency range from $10^{2.5}$ to 10^6 Hz. The crystalline sample was powdered with agate milk stick and

pelletized with a shaper. Gold paste (No. 8556, Tokuriki Chemical Research Co., Ltd.) and 30 μm ϕ gold wires (Nilaco Corp.) were used for electrical contacts between sample and electrical wire from the device. Temperature was controlled by water bath with pipe heater (AW-1105, Hakko Electric Co.,Ltd) and temperature controller (TC-3000A, As One). The impedance was measured in a closed glass cell containing a saturated KCl solution and humidity was monitored by humidity sensor (SHT31-DIS, Senserion). Data fitting is carried out by using EIS Spectrum Analyser.

3-6. References

1. R. Bashyam, P. Zelenay, *Nature*, **2006**, 443, 63-66.
2. R. Devanathan, *Energy Environ. Sci.*, **2008**, 1, 101−119.
3. A. Kraytsberg, Y. Ein-Eli, *Energy Fuel*, **2014**, 28, 7303−7330.
4. R. P. Bisbey, W. R. Dichtel, *ACS Cent. Sci.* **2017**, 3, 533−543.
5. A. I. Cooper, *ACS Cent. Sci.*, **2017**, 3, 544−553.
6. H. Zhang, P. K. Shen, *Chem. Rev.*, **2012**, 112, 2780− 2832.
7. M. Yoon, K. Suh, S. Natarajan, K. Kim, *Angew. Chem., Int. Ed.*, **2013***,* 52, 2688−2700.
8. S. Bureekaew, S. Horike, M. Higuchi, M. Mizuno, T. Kawamura, D. Tanaka, N. Yanai, S. Kitagawa, *Nat. Mater.*, **2009***,* 8, 831−836.
9. D. Umeyama, S. Horike, M. Inukai, T. Itakura, S. Kitagawa, *J. Am. Chem. Soc.*, **2012***,* 134, 12780−12785.
10. J. A. Hurd, R. Vaidhyanathan, V. Thangadurai, C. I. Ratcliffe, I. L. Moudrakovski, G. K. H. Shimizu, *Nat. Chem.* **2009**, 1, 705−710.
11. K. D. Kreuer, *Chem. Mater*., **1996**, 8, 610–641.
12. W. Weppner, K. D. Kreuer and A. Rabenau, *Angew. Chem. Int. Ed.*, **1982**, 122, 208–209.
13. Ramaswamy, N. E. Wong and G. K. H. Shimizu, *Chem. Soc. Rev*., **2014**, 43, 5913–5932.
14. C. J. Pedersen, *J. Am. Chem. Soc.*, **1967**, 89, 2495−2496.
15. C. J. Pedersen, *J. Am. Chem. Soc*., **1967**, 89, 7017−7036.
16. G. W. Gokel, W. M. Leevy, M. E. Weber, *Chem. Rev*., **2004**, 104, 2723−2750.
17. M. Bühl, G. Wipff, *J. Am. Chem. Soc*. **2002**, 124, 4473−4480.
18. K. M. Fromm, R. D. Bergougnant, *Solid State Sci*. **2007**, 9, 580− 587.
19. I. Hisaki, *J. Am. Chem. Soc.* **2016**, 138, 6617-6628.
20. P. Rought, C. Marsh, S. Pili, I. P. Silverwood, V. G. Sakai, M. Li, M. S. Brown, S. P. Argent, I. Vitorica-Yrezabal, G. Whitehead, M. R. Warren, S. Yang and M. Schröder, *Chem. Sci*., **2019**, 10, 1492–1499.
21. D.-W. Lim and H. Kitagawa, *Chem. Rev*., **2020**, 120, 8416–8467.
22. Y. Tian, G. Liang, T. Fan, J. Shang, S. Shang, Y. Ma, R. Matsuda, M. Liu, M. Wang, L. Li and S. Kitagawa, *Chem. Mater.*, **2019**, 31, 8494–8503.

23. Géraud Dubois, Catherine Reyé, Robert J. P. Corriu and Claude Chuit, *J. Mater. Chem.*, **2000**, 10, 1091–1098.

Chapter 4

C_3-Symmetric Hydrogen-bonded Organic Frameworks based on Tribenzo-18-Crown-6-ether Derivative

4-1. Abstract

In **Chapter 4**, the author successfully constructed the C_3-symmetric HOF **3CT-18C6-I** as designed, which was self-assembled by an 18-crown-6-ether (18C6) derivative with three dicarboxy-*o*-terphenyl moieties. Based on the previous analysis of pristine 18C6, it is obviously that the crown macrocycle has completely different conformation in HOF **3CT-18C6-I**. The molecule **3CT-18C6** has C_3-symmetry and the macrocyclic part includes an eclipsed conformation with small dihedral angle of the non-aromatic O–C–C–O moiety, on the other hand, activation of **3CT-18C6-I** causes low-symmetrization of the framework. The resultant framework **3CT-18C6-Ia** contains crystallographically independent two molecules of **3CT-18C6**, although each of them remains to be C_3-symmetric. The eclipsed conformation observed in the non-aromatic O–C–C–O moiety of **3CT-18C6-I** has been changed into the gauche conformation, which is energetically more stable. Interestingly, the HOF has 1D channels with a shish kebab like shape and the bottle neck part of the channel is consist of eclipse-stacked 18C6 macrocycles, which can provide fundamental insight of the proton conducting pass through the narrow 18C6 channel.

4-2. Introduction

Since it was found by by Pedarsen in 1967,[1] crown ethers have been one of the most important ionophores in host-guest and supramolecular chemistry because of its highly-selective recognition ability toward specific cationic and molecular species caused by preorganized oxygen atoms in the macrocycle. A number of molecular systems incorporated by crown ethers with various size have been developed and their functionality and intensively investigated in solution, liquid crystal, and solid states.[2]
A crystalline porous framework composed of crown ether building blocks is also attractive for us because, in such porous frameworks, functional crown ether moieties can ideally arrange with precise periodicity and orientation, and furthermore, guest molecules or analytes are capable of accessing to the crown ether through the channel spaces. Indeed, metal-organic frameworks (MOFs),[3] and covalent organic frameworks (COFs)[4] composed of crown ether building blocks were reported. Especially, Shu and coworkers demonstrated that the MOFs incorporating crown ether showed the improved hydrogen uptake depending on cations inserted in the crown ether moiety. However, such frameworks are very limited probably because of high flexibility and various low-symmetric conformations of the crown ether moiety.[5] Particularly, there is no example of crown ether-based hydrogen-bonded organic frameworks (HOFs). HOFs are porous molecular crystals, in which building block molecules are connected and organized through intermolecular hydrogen-bonds.[6] Reversible H-bonds can provide highly-crystalline HOFs, which can be easily reproduced by simple recrystallization repeatably. The nature of H-bonds, however, makes the framework fragile and difficult to construct as it was designed. Therefore, highly-symmetric rigid molecules such as pi-conjugated polycyclic aromatic hydrocarbons composed of sp and sp^2 carbon atoms are preferable as building block molecules to construct HOFs.[7] The structural features required by the building block molecules are completely opposite to those of crown ethers. Indeed, we recently constructed proton conductive HOFs based on

dibenzo18crown-6-ether, which, however, have very complex structures with no porosity.[8]

Keeping this in mind, the author newly designed 4,4'-dicarboxy-o-terphenyl (CT) subsitited 18crown-6-ether derivative (3CT18C6) as shown in Figure 4-1. Although pristine tribenzo18-crown-6 is not flat but has boat-shaped conformation in crystalline state as reported by Bryan,[10] we expected that incorporation of the CT groups in 18C6 provides symmetric porous HOF with porosity by a rigid spacer and highly-directional and predictable H-bonding between the carboxy groups. Herein, we demonstrate that 3CT18C6 form a C_3-symmetric rigid crystalline HOF. This is the first example of a rigid HOF composed of flexible crown ether derivatives. It is noteworthy that the HOF has one-dimensional (1D) channels with a shish kebab like shape and the bottle neck part of the channel is consist of eclipse-stacked 18C6 macrocycles. This HOFs can provide fundamental insight of the proton conducting pass through the narrow 18C6 channel.

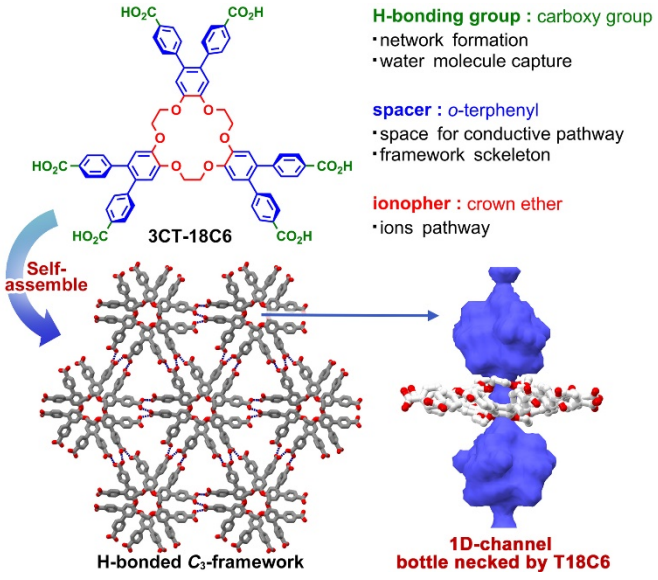

Figure 4-1. Concept and overview of this study. Construction of porous HOFs composed of armed crown ether derivative **3CT-18C6**.

4-3. Results and discussion.

Synthesis and Characterization.

The synthetic route of **3CT-18C6** refers to **Chapter 2**. With the synthesized molecular building block, we explored various crystallization conditions to obtain a HOF. Previously reported conditions that resulted in formation of HOFs have not given any single crystalline materials of 3CT-18C6. However, we finally found that slow evaporation of a mixed solution of DMF, H_2O, EtOH and 2M HCl (v/v = 2/0.5/0.3/0.05) at 80 °C afforded a HOF **3CT18C6-I** as colorless crystals.

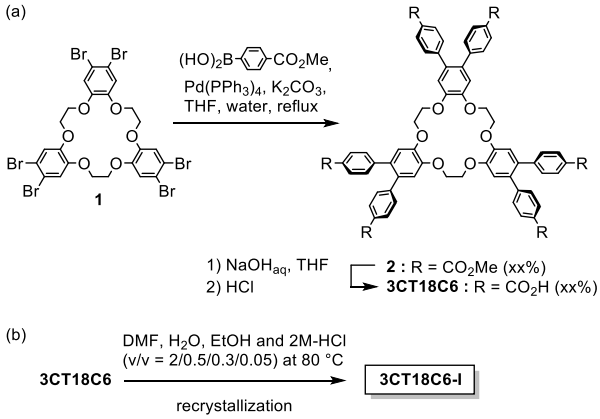

Scheme 4-1. (a) Synthesis and (b) crystallization of building block molecule.

Single crystal X-ray diffraction reveals that **3CT-18C6** crystallizes in trigonal space group *R*-3 to form HOF **3CT-18C6-I**. The molecule has three-fold axis at the center of the macrocycle. The oxygen and sp^3-carbon atoms in the macrocycle are disordered in two positions with an occupancy of 0.75 : 0.125. Two molecules of **3CT-18C6** form a stacked dimer, in which the molecules are rotated by 60 degree, and therefore, the macrocycle moieties are arranged in the eclipsed fashion to form a 1D ionopher channel. The peripheral phenylene groups, whose dihedral angles against the benzene ring incorporated in T18C6 is 36.62° and 60.24°, are alternately contacted to those in the other molecule with contact angle of 49.51°, which is typical face-to-edge interaction observed in the crystal of aromatic molecules and stabilize the dimer. The dimer has a small cavity in which one water molecule is accommodated.

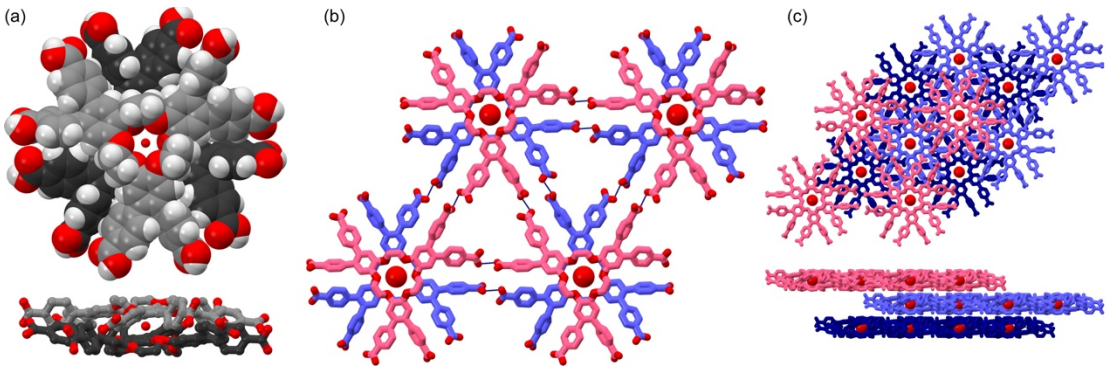

Figure 4-2. Crystal structure of **3CT-18C6-I.** (a) Spacefilled plot along *c* axis. (b) Hydrogen bonds among carboxy groups. (c) Packing diagram along *c* axis. (d) Packing diagram along *a* axis. water molecule was colored with red.

The dimers are connected through truncated H-bonds between the carboxy groups with a O…O distance of 2.596 Å and dihedral angle of 49.34° to form 2D hexagonal network. The 2D networks are stacked in an ABC fashion with interlayer distance of 3.267 Å to give the layered framework. The hexagonal networks included two types of voids. The smaller triangular one was formed with 16.538 Å on a side and a diameter of 13.184 Å and the lager void was formed with alternate sides of 24.677 Å and a diameter of 21.669 Å, which accommodated solvent guest molecules such as DMF and ethanol. The potential solvent accessible void space accounts for approximately 19.7% of the whole crystal volume as estimated by PLATON.[9]

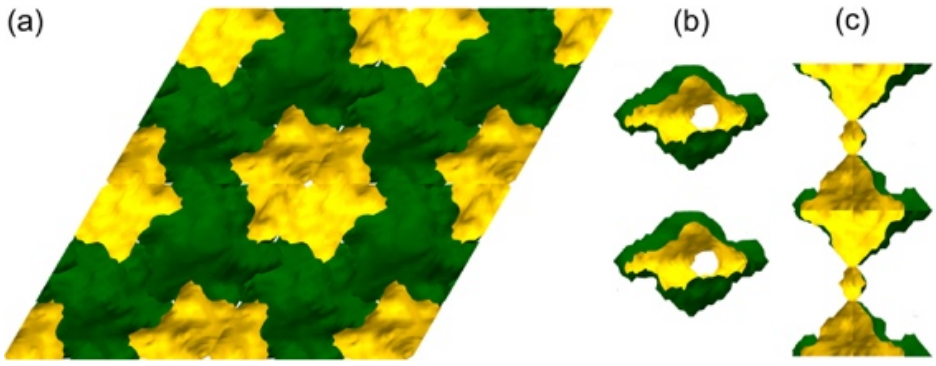

Figure 4-3. Two types viods of **3CT-18C6**.

The powder X-ray diffraction (PXRD) patterns of as-synthesized **3CT-18C6-I** is in good agreement with the simulated pattern, indicating high phase purity and good stability of **3CT-18C6-I** in bulk amount (Figure 4-4). The thermogravimetric analysis (TGA) suggested the framework of **3CT-18C6-I** maintains after losing guest molecules step by step from the room temperature (Figure 4-5). On the other hand, DTA analysis indicated the phase transformation.

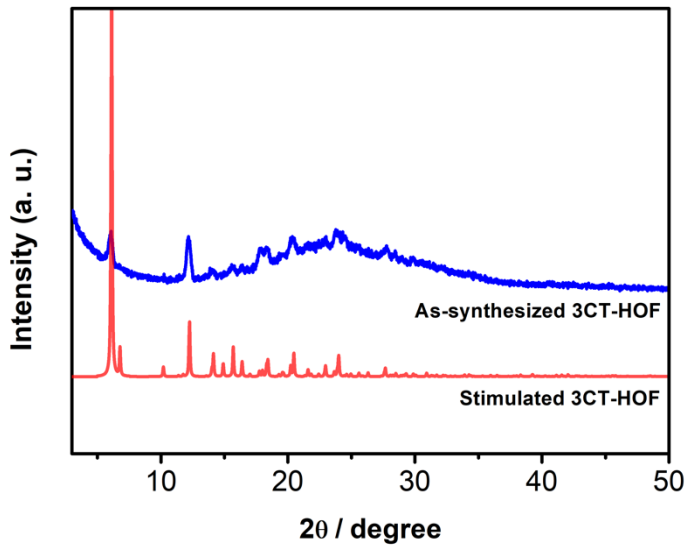

Figure 4-4. PXRD pattern of **3CT-18C6-I**.

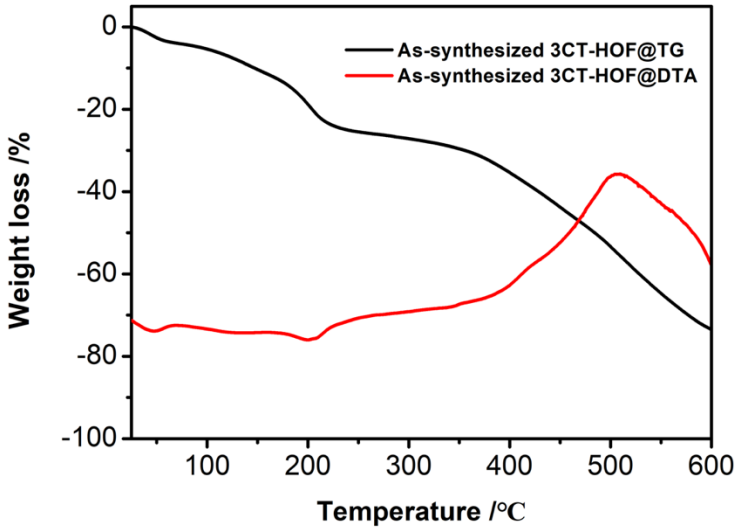

Figure 4-5. TG plot of **3CT-18C6-I**.

Activation of **3CT-18C6-I** was measured under the condition for 160 °C in the vacuum for 1 day. Interestingly, the structure of the activated HOF **3CT-18C6-Ia** was able to be revealed by SCXRD analysis. The space group was slightly changed from R-3 to R3c. The crystal consists of crystallographically independent two molecules A and B, both of which have a C_3-axis at the center of the T18C6 ring. The molecular packing manner is basically the same with that of **3CT-18C6-I**, while the rotation angles between the peripheral phenylene group and the benzene ring of the T18C6 moiety were changed into 41.75° and 54.97° for molecule A and 48.37° and 53.55° for molecule B. The different rotational angles result in the different H-bonding manners of the terminal carboxy groups as shown in Figure 4-6. A water molecule is located at the middle of the T18C6 dimer, additionally, other molecules of water, which are disordered in several positions, are also solved crystallographically. In the structure, two types of voids are aligned along the x axis. One has 1D channel void composed of large and small spherical voids. The other looks similar with the former, while each of void spaces is almost discrete.

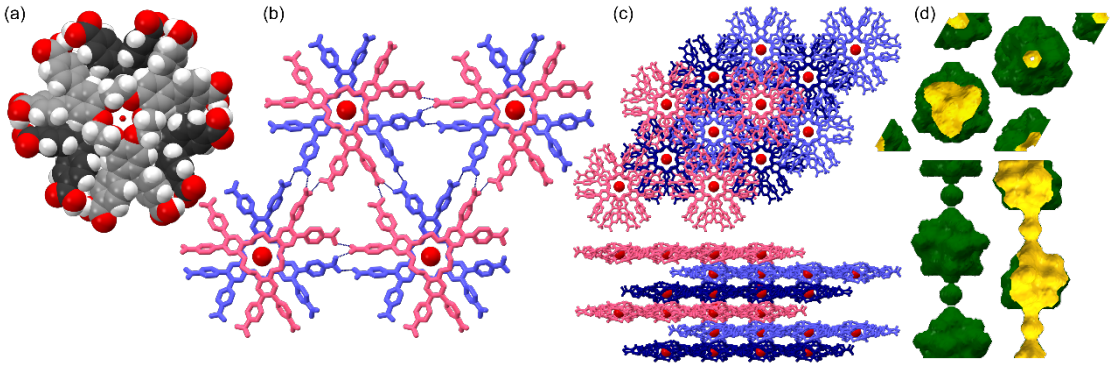

Figure 4-6. Crystal structure of **3CT-18C6-Ia.** (a) Spacefilled plot along *c* axis. (b) Hydrogen bonds among carboxy groups. (c) Packing diagram along *c* and *a* axis. (d) Two types of voids of **3CT-18C6-Ia.** water molecule were colored with red.

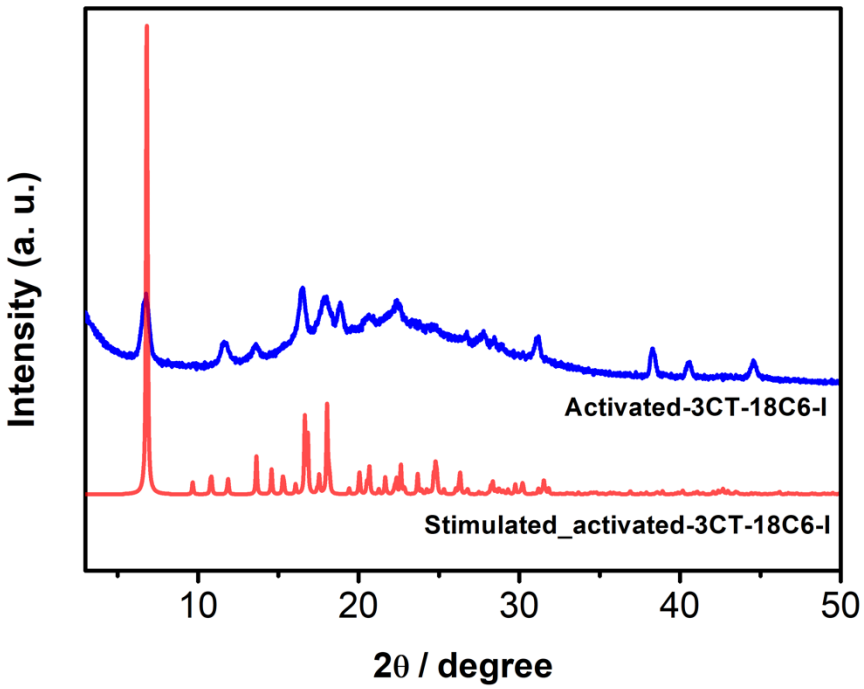

Figure 4-7. PXRD pattern of **3CT-18C6-Ia**. PXRD patterns of crystalline bulk samples of **3CT-18C6-Ia** is in good agreement with the simulated from single-crystal data, indicating high phase purity and good stability.

For deeper insight for the structural changes, conformations of the 18C6 moiety was carefully compared among, pristine 18C6, Br_6-T18C6, **3CT-18C6-I** and **3CT-18C6-Ia**. Pristine 18C6 molecule is a flexible molecule and have many possible conformations. Conformation of 18C6 was thoroughly explored by theoretical calculations both in vacuo[10] and in solvents such as acetonitrile.[11] Wipff showed that 12 conformers of 18C6 with the larger occurrence after a 2-ns MD simulation in acetonitrile and D_{3h} conformer is the most dominant. In the case of T18C6, a dihedral angle of three O–C(arom)–C(arom)–O moieties is fixed to be ca. 0°, where C(arom) denotes the carbon atom in the part of benzene ring, resulting in that possible conformations should be reduced compared with 18C6. The above-mentioned conformational restriction, however, is expected to make it difficult for T18C molecule to have highly-symmetric planar conformations such as a D_{3h}-symmetric one. Indeed, the hitherto known crystal structure of pristine T18C6, reported by Bryan and coworkers as an acetonitrile disolvate,[5] shows a low-symmetric boat-shaped

conformation represented by 0aa g+aa 0ag+ g+aa 0 aa g-aa as shown in Table 4-2 and Figure 4-8a, where “g” and “a” represent gauche and anti, respectively, “0” represents an aromatic O–C(arom)–C(arom)–O torsion angle, and a superscript following the “g” indicates the sign of the angle. Hexabromotribenzo-18-crown-6 also shows a similar boat-shaped conformation represented by [0aa g^{+}aa 0aa $g^{-}g^{-}$a 0 aa g^{-}aa] (Figure 4-8b).

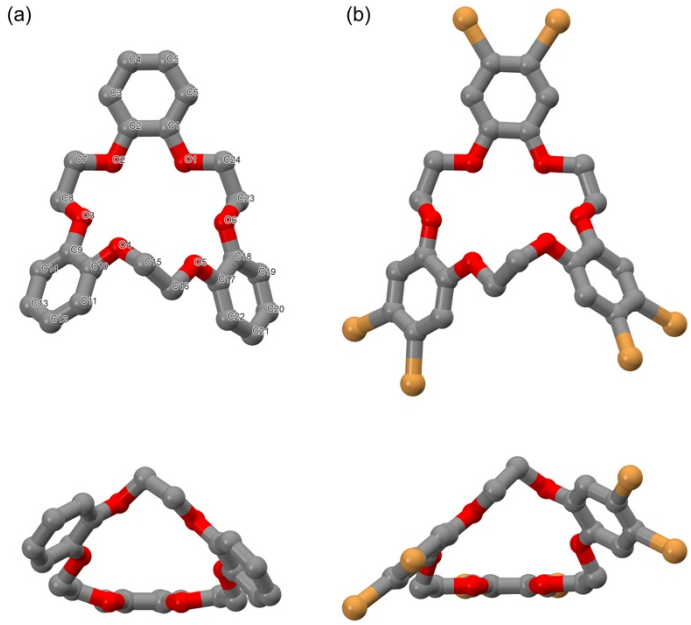

Figure 4-8. Conformation of the crown ether moiety in (a) T18C6-acetonitrile disolvate and (b) Br_4T18C6.

In the case of HOF **3CT-18C6-I**, on the other hand, the crown macrocycle has completely different shape. The molecule **3CT-18C6** has C_3-symmetry and the macrocyclic part includes an eclipsed conformation with small dihedral angle of non-aromatic O–C–C–O moiety. The total confirmation is represented by [0aa e(or g^{+})aa 0aa e(or g^{+})aa 0aa e(or g^{+})aa]. This conformation provides the molecule relatively flat molecular shape (Figure 4-9).

Activation of **3CT-18C6-I** causes low-symmetrization of the framework. The resultant framework **3CT-18C6-Ia** contains crystallographically independent two molecules of **3CT-18C6**, A and B, although each of them remains to be C_3-symmetric. It is noteworthy that the eclipsed conformation observed in non-aromatic O–C–C–O

moiety of **3CT-18C6-I** has been changed into the gauche conformation, which is energetically more stable. The conformations of the A and B molecules are represented by [0aa g^-aa 0aa g^-aa 0aa g^-aa] and [0aa g^+ag^+ 0aa g^+ag^+ 0aa g^+ag^+]. However, the total molecular shape retains flat similar with that in **3CT-18C6-I**.

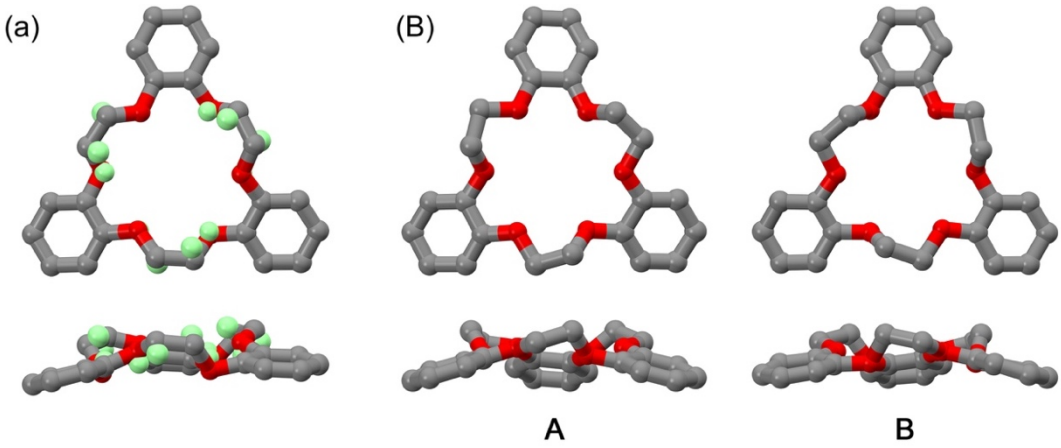

Figure 4-9. Conformation of the crown ether moiety in (a) **3CT18C6-I** and (b) **3CT18C6-Ia**. Disordered atoms in (a) are shown in light green spheres.

Therefore, the carboxyphenyl moieties introduced in the macrocycle crucially control its conformation through intermolecular H-bonds.

Crystallography

Table 4-1. Crystallographic parameters of **3CT-18C6-I** and **3CT-18C6-Ia**.

Identification code	**3CT-18C6-I**	**3CT-18C6-Ia**
Crystal color and shape	colorless, block	yellow, block
Empirical formula	$C_{66}H_{48}O_{18.5}$	$C_{132}H_{98}O_{40.5}$
Formula weight	1137.05	2332.12
Temperature/K	293(2)	222(2)
Crystal system	trigonal	trigonal
space group	R-3	R3c
a / Å	26.0511(11)	25.7783(6)
b / Å	26.0511(11)	25.7783(6)
c / Å	18.7773(15)	31.8836(17)
α / °	90	90
β / °	90	90
γ / °	120	120
V / Å^3	11036.2(13)	18348.7(13)
Z	6	6
ρ_{calc} / g cm^{-3}	1.026	1.266
μ / mm^{-1}	0.630	0.793
F (000)	3552.0	7284.0
Radiation	1.54184	1.54184
2θ max /°	144.936	145.174
Reflections collected	12930	11390
Independent reflections	4717	5831
Goodness-of-fit on F^2	1.079	1.067
Final R indexes [I>=2σ (I)]	R_1 = 0.0716, wR_2 = 0.2315	R_1 = 0.0887, wR_2 = 0.2309

Table 4-2. Dihedral angles and conformation of the crown ether moiety in crystals of T18C6 and its derivatives[a,b]

	T18C6[c]	Br_6-T18C6	**3CT18C6-I**[d]	**3CT18C6-Ia** A[e]	**3CT18C6-Ia** B[e]
O1-C1-C2-O2	0.45 (0)	−2.30 (0)	3.42 to 25.72 (0)	0.46 (0)	-1.49 (0)
C1-C2-O2-C7	159.27 (a)	−178.74 (a)	−148.51 to −171.50 (a)	-127.65 (a)	-174.52 (a)
C2-O2-C7-C8	−17.50 (a)	178.12 (a)	−143.63 to −177.68 (a)	-144.34 (a)	-178.57 (a)
O2-C7-C8-O3	66.12 (g^+)	62.20 (g^+)	1.39 to 64.13 (e, g^+)	-52.99 (g^-)	61.97 (g^+)
C7-C8-O3-C9	173.57 (a)	−169.69 (a)	136.43 to 176.94 (a)	179.67 (a)	155.34 (a)
C8-O3-C9-C10	−179.33 (a)	153.80 (a)	102.82 to 124.71 (a)	178.36 (a)	106.57 (g^+)
O3-C9-C10-O4	0.90 (0)	2.02 (0)			
C9-C10-O4-C15	−169.91 (a)	178.83 (a)			
C10-O4-C15-C16	76.59 (g^+)	−174.59 (a)			
O4-C15-C16-O5	65.79 (g^+)	−72.43 (g^-)			
C15-C16-O5-C17	−172.70 (a)	-69.13 (g^-)			
C16-O5-C17-C18	167.73 (a)	157.15 (a)			
O5-C17-C18-O6	0.79 (0)	−1.32 (0)			
C17-C18-O6-C23	−172.59 (a)	−172.40 (a)			
C18-O6-C23-C24	178.30 (a)	−170.01 (a)			
O6-C23-C24-O1	−69.35 (g^-)	−58.82 (g^-)			
C23-C24-O1-C1	−176.70 (a)	172.68 (a)			
C24-O1-C1-C2	−169.94 (a)	−176.86 (a)			

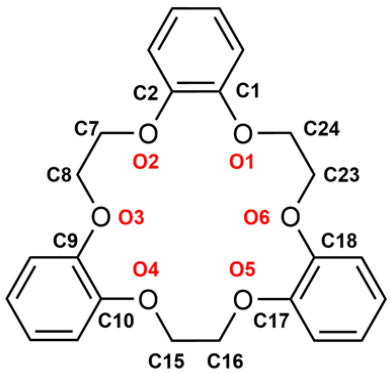

[a] The crystal structure was reported as a solvate of acetonitrile, see ref 10.

[b] Conformations are shown in the parentheses.

[c] Since molecules in the crystals are C_3-symmetry, dihedral angles of a third part of the molecules are shown.

[d] Since the atomic positions of the crown ring are disordered in two position, dihedral angles also have a range.

[e] **3CT18C6-Ia** contains crystallographically independent two molecules A and B.

Gas sorption

The porous nature of **3CT-18C6-Ia**, as revealed by its crystal structure, encouraged me to examine its permanent porosity through the gas sorption studies. The BET surface area of **3CT-18C6-Ia** derived from the N_2 isotherm is 8.8 m^2 g^{-1}. The experimental pore volume is 2.02 cm^3 g^{-1}, based on the test condition as shown in Figures 4-10.

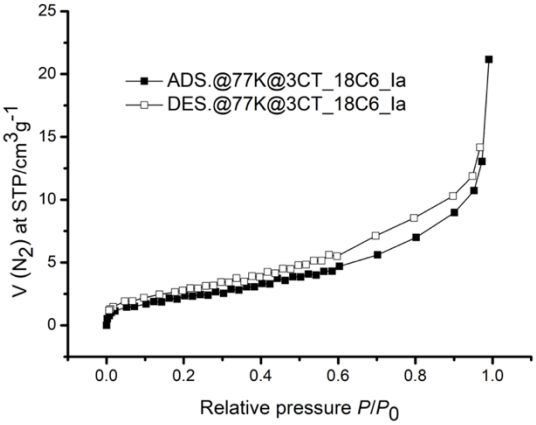

Figure 4-10. N_2 adsorption/desorption isothermal of **3CT-18C6-Ia**.

In addition, the adsorption isotherm for CO_2 measured at 195 K show that the **3CT-18C6-Ia** adsorption are 76.5 cm^3 g^{-1} (Figures 4-11), demonstrating this structure as the good HOF material for potential carbon dioxide capture and separation. Moreover, the BET surface area of 3453.0 m^2 g^{-1} between relative pressure of 0.24 and 0.34 kPa (Figures 4-11).

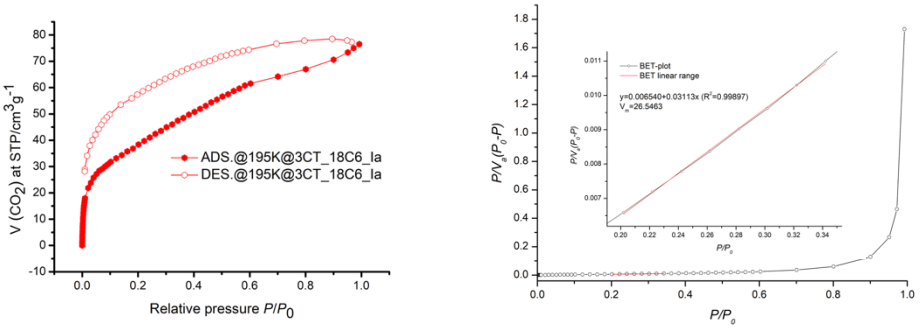

Figure 4-11. CO_2 adsorption/desorption isothermal and BET-plot with linear range of filled circles of **3CT-18C6-Ia**.

I also performed H_2O adsorption isotherm where **3CT-18C6-Ia** showed a relatively uptake of 6.5 mmol g^{-1} (Figures 4-12). This result indicates that at higher RH/relative pressure the structures show gate opening behavior probably to accommodate number of H_2O molecules inside the framework expected to show proton conductivity.

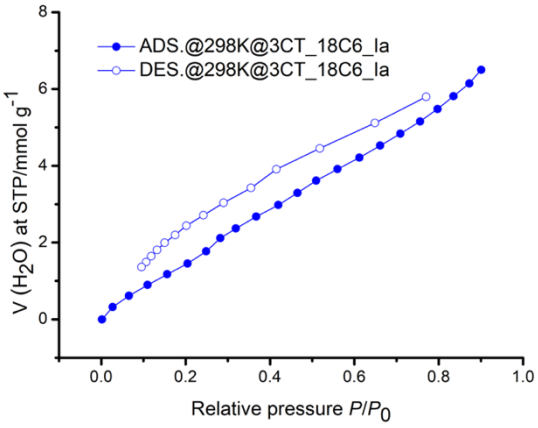

Figure 4-12. Water adsorption/desorption isothermal of **3CT-18C6-Ia**.

Proton Conductivity.

The structures of **3CT-18C6-Ia** was constructed by hydrophilic crown ether moiety, assembly of carboxy groups, involved 1D channel for water molecules which supplied at higher relative humidity. These structural features could provide an orderly way for proton transport. Therefore, **3CT-18C6-Ia** is expected to show proton conductivity. Due to the limitation of the size of the samples, compressed pellet of the samples was used for the measurement for proton conductivity.

Temperature-dependent Nyquist plots[20–22] and the fitting parameters of equivalent circuit model for **3CT-18C6-Ia** under different relative humidity were summarized in Figures 4-13, 14, respectively.

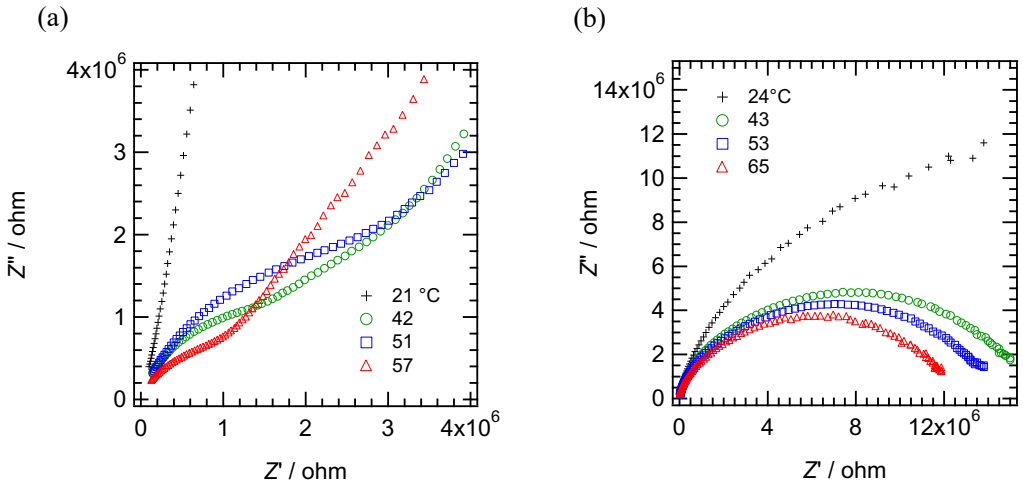

Figure 4-13. Nyquist plots of **3CT-18C6-Ia** with different temperature (a) under 85% RH and (b) 98% RH, respectively.

The Nyquist plots of **3CT-18C6-Ia** was the sum of a straight line and a semicircle in the low and high frequency range under 85% RH and 98% RH, respectively. Since the pellet sample was used to measure the proton conductivity, the Nyquist plot showed the proton conductions which are contributed from a bulk and an interface. Since bulk conduction is usually observed in the higher frequency range than the interface[12–13] the semicircles in the Nyquist diagram of **3CT-18C6-Ia** was attributed to bulk conduction.

For the calculation of proton conductivity, the author applied the equivalent circuit model.

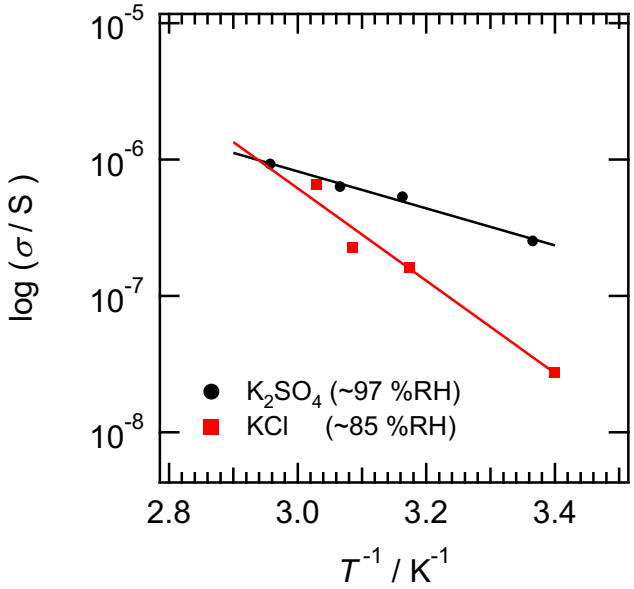

Figure 4-14. Arrhenius plot for proton conductivities of **3CT-18C6-Ia** under 85 %RH (red) and 98 %RH (black), respectively.

Regarding the conductivity estimated from the equivalent circuit model, an Arrhenius plot was created from the bulk conductivity of **3CT-18C6-Ia** (Figure 4-14). From the Nyquist plots, the proton conductivities of **3CT-18C6-Ia** increased with the increasing temperature under the different relative humidities, and **3CT-18C6-Ia** show the highest proton conductivity of 6.36×10^{-6} S cm^{-1} at 330 K under 85 %RH, and 2.58×10^{-5} S cm^{-1} at 338 K under 98 %RH, respectively. In addition, from the Arrhenius plot, It is notable that the E_a decreased with the increasing relative humidity which shows that **3CT-18C6-Ia** were 0.64 eV under 85 %RH and 0.27 eV under 98 %RH. Referring to the proton diffusion motion, the mechanism of proton conducting can be classified as vehicle and Grotthuss mechanism. Previously reported of the structure of **3CT-18C6-Ia**, there was an 1D channel in the framework which offered the space for water molecules supplied by the higher relative humidity. Moreover, at higher relative humidity/relative pressure this structure show gate opening behavior probably to accommodate more number of H_2O molecules inside the framework correlating to the

fact that higher conductivity value at higher relative humidity and corresponding to the Grothuss mechanism.

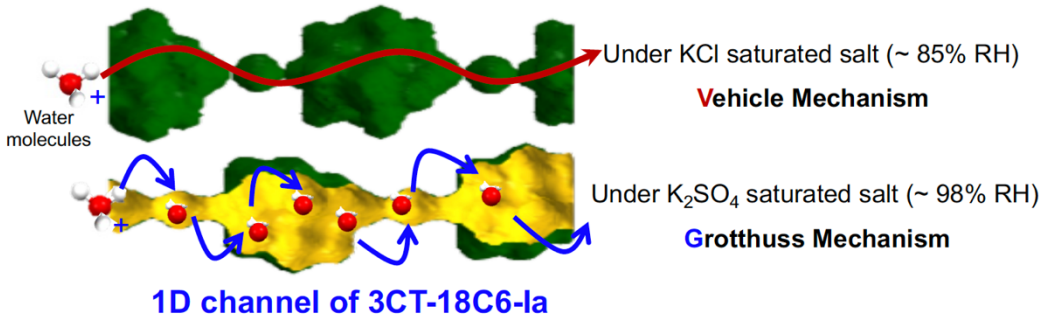

Figure 4-15. 1D channel of **3CT-18C6-Ia** for proton conducting.

4-4. Conclusion

The author successfully constructed the C_3-symmetric HOF **3CT-18C6-I** as designed, which was self-assembled by 18-crown-6 ethers with three *o*-bis(4-carboxyphenyl)aryl moieties. This is the first example of a rigid HOF with permanent porosity composed of flexible crown ether derivatives. It is noteworthy that after activation, the **3CT-18C6-Ia** has one-dimensional (1D) channels with a shish kebab like shape and the bottle neck part of the channel is consist of eclipse-stacked 18C6 macrocycles. This HOF exhibits the proton conduction through the narrow 18C6 channel.

4-5. Measurement

Thermogravimetric analysis (TGA) was conducted using a Rigaku Thermo Plus TG8120 with a heating rate of 5 K/min under nitrogen.

PXRD were measured with a Rigaku RINT2100 in the 2θ region of 5–50°. The measurements were performed with Cu K_α radiation (λ = 1.5418 Å) at scanning rate of $1.2° \cdot \mathrm{min}^{-1}$ under an applied electric voltage and current of 40 KV and 40 mA, respectively.

Single crystalline X-ray diffraction data was collected by Rigaku MicroMax-007HF diffractometer with a Pilatus 200K detector and Cu K_α radiation (λ = 1.54184 Å) at 223K. Analytical and multi-scan absorption corrections were applied to the reflection data. A single crystal was mounted on MicroMounts™ tip (MiTeGen) with Paratone® 8277 (Hampton Research). Data collection, cell refinement, and data reduction were carried out with Crysalis ^{PRO} (Rigaku Oxford Diffraction, 2017). The initial structure was solved by using SHELXT, and structural refinement was performed by using full-matrix least-squares techniques on F^2 using Crystal structure software (Rigaku). Anisotropic refinement was applied to all atoms except for hydrogens. SQUEEZE function equipped in the PLATON program was used to remove severely disordered solvent molecules in voids.

4-6. Reference

1. C. J. Pedersen , *J. Am. Chem. Soc.*, **1967**, 89, 7017.
2. a) F. T. H. Leuwerink, W. J. Briels, *J. Chem. Soc.*, **1995**, 103, 4637. b) F. T. H. Leuwerink, W. J. Briels, *J. Phys. Chem.*, **1995**, 99, 16549.
3. D.-W. Lim, A. -C. Seung, P. S. Myunghyun, *Angew. Chem. Int. Ed.*, **2014**, 53, 7819-7822.
4. S. H. An, Q. Xu, Z. H. Ni, J. Hu, C. J. Peng, L. P. Zhai, Y. Guo, H. L. Liu, *Angew. Chem. Int. Ed.*, **2021**, 60, 9959-9963
5. N. A. Jallal, A. A. Kahtani, A. A. Azhary, *J. Phys. Chem. A.*, **2005**, 109, 3694-3703.
6. A.G. Slater, A.I. Cooper, *Science*, **2015**, 348, aaa8075.
7. I. Hisaki, *Journal of Inclusion Phenomena and Macrocyclic Chemistry*, **2020**, 96, 215–231.
8. Previous work (**Chapter 2**)
9. A. L. Spek., *J. Appl. Cryst.*, **2003**, 36, 7-13.
10. J. C. Bryan, N. L. Engle, R. A. Sachleben, B. P. Hay, *Acta crystallogr. C*, **2001**, 57, 1359-1360.
11. L. Troxler, G. Wipff, *J. Am. Chem. Soc.*, **1994**, 116, 1468.
12. P. Rought, C. Marsh, S. Pili, I. P. Silverwood, V. G. Sakai, M. Li, M. S. Brown, S. P. Argent, I. Vitorica-Yrezabal, G. Whitehead, M. R. Warren, S. Yang and M. Schröder, *Chem. Sci*., **2019**, 10, 1492–1499.
13. D.-W. Lim and H. Kitagawa, *Chem. Rev*., **2020**, 120, 8416–8467.

Chapter 5

Summary and Perspectives

In **Chapter 2**, the author reported the synthetic routes of the surveyed sython, as 1CT-18C6, 2CT-18C6, 2CT-24C8, and 3CT-18C6, in detail. Besides characterizations exhibited the good purity of each compound, which show important effect through this study.

In **Chapter 3**, the author constructed various organic frameworks base on 1CT-18C6 and 2CT-18C6. It is noteworthy that the carboxy groups form no self-complementary dimer, which is often observe in hydrogen bonded frameworks composed of highly-symmetric rigid π-conjugated molecules. This result clearly indicates that flexibility and lower symmetry of **2CT-18C6-I, II, III** crucially effects on a way of formation of a hydrogen bonded network. However, the carboxy groups of **2CT-18C6-III** form hydrogen bonds with only water molecules to give the crystal contains no solvent but water molecules which form one-dimensional zig-zag alignment along the *c* axis interestingly. Additionally, the unique water pathway provide available space for H^+ which result in the proton conductivity of **2CT-18C6-III.**

In **Chapter 4**, the author successfully constructed the C_3-symmetric HOF **3CT-18C6-I** as designed, which was self-assembled by 18-crown-6 ethers with three *o*-bis(4-carboxyphenyl)aryl moieties. Based on the previous analysis of pristine 18C6, it is obviously that in the case of HOF **3CT-18C6-I**, the crown macrocycle has completely different shape. The molecule **3CT-18C6** has C_3-symmetry and the macrocyclic part includes an eclipsed conformation with small dihedral angle of non-aromatic O–C–C–O moiety, on the other hand, activation of **3CT-18C6-I** causes low-symmetrization of the framework with permanent porosity which applies enough space for water molecules supplied by the higher relative humidity to achieve proton conduction.

In summary, in this thesis, the author newly designed, 1CT-18C6, 2CT-18C6 and 3CT-18C6, as building blocks to construct a series of proton conductive crystalline frameworks. It is notable the proton conductivity increasing followed the order from **1CT-18C6-I**, **2CT-18C6-III** to **3CT-18C6-Ia**, as expected. Therefore, the author

believes that this study provides a new strategy of development of proton conductive HOFs composed of crown ethers.

List of Publications

1. Designing Hydrogen-Bonded Organic Frameworks (HOFs) with Permanent Porosity. *Angew. Chem. Int. Ed.*, **2019**, 58, 11160–11170
   Ichiro Hisaki, Chen Xin, Kiyonori Takahashi, Takayoshi Nakamura
2. A Proton Conductive Framework Incorporating 18Crown-6-ether and Dicarboxy-*o*-terphenyl Moieties
   Xin Chen, Kiyonori Takahashi, Kenta Kokado, Takayoshi Nakamura, Ichiro Hisaki
   just accepted
3. C_3-Symmetric Hydrogen-bonded Organic Frameworks based on Tribenzo-18-Crown-6-ether Derivative
   Xin Chen, Rui-Kang Huang, Kiyonori Takahashi, Takayoshi Nakamura, Ichiro Hisaki
   on praperation